EUROPEAN ORGANIZATION FOR NUCLEAR RESEARCH

NP/Int-Rep. 72-4

VERY HIGH ENERGY STRONG INTERACTIONS

by

J.V. Allaby

CERN, Geneva

15th December 1971

Invited paper presented at the Conference on Particle Physics, University of California, Irvine, on December 3-4, 1971.

1. Total Cross-Sections

During the last two years, a number of measurements of total cross-sections have been made at the 70 GeV accelerator at the Institute for High Energy Physics (IHEP) Serpukhov, USSR. The earliest measurements [1] were for negative particles only and for technical reasons had to be carried out using a high pressure gas target, rather than the usual and more precise liquid targets. These early measurements on hydrogen and deuterium were followed by measurements on a liquid target [2] but only of hydrogen and also limited to negative particles. More recently, a positive beam was constructed which enabled measurements to be made of total cross-sections for π^+, K^+ and protons on both liquid hydrogen and liquid deuterium targets [3]. The final phase of these measurements is under way at Serpukhov now, and is a re-measurement of negative particle total cross-sections on both hydrogen and deuterium liquid targets using the identical targets used earlier this year in the measurements on positive particles.

It is useful perhaps to review what we have learned from the measurements so far. Since the data on hydrogen targets for both positive and negative particles are quite precise, it is possible to compare the behaviour of particle and antiparticle cross-sections. The data are shown in Figure 1, which is a compilation of total cross-section data on hydrogen. The $\bar{p}p$ total cross-section is seen to continue falling in magnitude with increasing energy all the way up to the highest energy measured. On the other hand the pp total cross-section is seen to change from a gentle fall off with energy up to 35 GeV/c to a rather constant value of about 38.45 mb above 40 GeV/c.

The $\pi^{\pm}p$ total cross-sections seem to show a rather energy independent behaviour above 35 GeV/c although there is a weak indication that the π^+p total cross-section might be starting to increase above 60 GeV/c. The K^-p total cross-section is virtually constant above 35 GeV/c but the K^+p total cross-section shows an unexpected rise in magnitude,

after being rather constant in the range 10-20 GeV/c. The flatness of the K^-p total cross-section, together with the constancy of the K^+p cross-section up to 20 GeV/c, led to speculation on the validity of the Pomeranchuck theorem before the K^+p data were available. However, the rising of the K^+p cross-section is adequate to satisfy the Pomeranchuck theorem as can be seen more clearly in Figure 2 which displays the differencies between particle and antiparticle cross-sections as a function of the incident momentum. The cross-section differences are all tending asymptotically to zero as demanded by the Pomeranchuck theorem.

The behaviour shown by the data of Figure 1 was not anticipated by simple Regge theory but the cross-section differences of Figure 2 are not too different from the predicted values. The major difference with conventional Regge fits lies in the momentum dependence of the difference cross-section $\Delta\sigma(\pi^{\pm}p)$, where the slope is flatter than expected from the usual exchange ideas. The reasons for this behaviour are not clearly understood, even though the early data of Foley et al.[4] had already shown the same energy dependence.

Lipkin [5] has recently pointed out that the data of Figure 2 are consistant with the requirements of ω universality, which says that the coupling of the ω trajectory to non-strange quark constituants should be a universal parameter. This results in a simple prediction for the total cross-sections on deuterium which isolates purely isoscaler exchange. The prediction is that :

$$\Delta\sigma(p^{\pm}d) = 3\Delta\sigma(K^{\pm}d) \qquad (1)$$

Lipkin uses the additional assumption that the isovector exchange, which carries the quantum numbers of the ρ trajectory, is universally coupled to the isospin current. The ρ couplings to kaons and nucleons are thus equal, and the coupling to pions is twice as strong as either. The combination of ω universality and ρ universality lead to the relation :

$$\Delta\sigma(p^{\pm}p) = 3\Delta\sigma(K^{\pm}p) - \Delta\sigma(\pi^{\pm}p) \qquad (2)$$

which is in excellent agreement with the data shown in Figure 2. Although one does not yet have the most precise data on negative particle total cross-sections, one can also look directly at the prediction of Equation 1, using the early data of the CERN-Serpukhov collaboration on gaseous targets. The difference between the left-and right-hand sides of Equation 2 is shown in Figure 3, where the band around zero represents the systematic scale error and the error bars on each point represent the contribution of the statistical errors on the cross-section differences. Within the errors one sees that ω-universality is good up to 50 GeV/c, which is perhaps surprising in view of the unexpectedness of the energy behaviour of the individual cross-sections themselves. The validity of Equation 2 thus supports not only ω-universality but also the ρ-universality assumed by Lipkin. The more precise data, to be provided soon, on the deuterium cross-sections will improve greatly the validity of these tests.

2. Boson Production at High Energies

I will now turn to another experiment still in progress at Serpukhov carried out by a collaboration between IHEP and the CERN Boson Spectrometer Group [6]. They have been studying the production and decay of negatively charged boson resonances initiated by pion-nucleon interactions. In the familiar nomenclature one can express this as :

$$\pi^- p \rightarrow X^- p \quad \hookrightarrow n\pi \qquad (3)$$

The data I shall present is preliminary and as yet unpublished. In addition to the general study of boson resonances the group have also obtained, as a by-product, some information on elastic scattering. Here again the data I will present is preliminary and represents only a fraction of the total data which they will have available when the analysis is complete.

The experiment uses equipment already used for some years at CERN to study reactions of the type represented by Equation 3. The layout of the experimental equipment is shown in Figure 4. The recoil proton produced in the reaction is detected at large angles and its energy and angle are

measured by means of a range telescope and spark chambers respectively. This information determines the mass of X^-. The decay products of X^- are separately determined by the spark chambers and magnetic spectrometer located near the forward directions.

At low energies the mass spectrum of X^- was found to be very rich in resonances as shown by the data compilation of Figure 5. However, at higher incident momenta, the picture looks quite different as shown in Figure 6, where the $(\text{mass})^2$ spectrum for X^- produced by incident pions of momentum 25 GeV/c and 40 GeV/c is shown. This data has been collected of the range of four momentum transfers squared, t, of $0.17 < |t| < 0.35$ GeV^2. Clearly at high masses (> 2 GeV) no structure is present. For a narrow resonance, an upper limit of the differential cross-section of 3 μb/GeV^2 is quoted by the authors. At low masses (< 2 GeV), apart from elastic scattering, a very pronounced peak is seen at 1.3 GeV, fitting the parameters of the A_2. The resolution of the apparatus at a mass of 2.5 GeV was $\Gamma_{X^-} = 40$ MeV (FWHM) at 25 GeV/c incident momentum and $\Gamma_{X^-} = 60$ MeV (FWHM) at 40 GeV/c, so no structure should be seen in the bump at 1.3 GeV, even if it does happen to be a split A_2. The major contribution to the mass resolution comes from the multiple scattering of the slow recoil proton.

The mass squared scale of Figure 6 was chosen in order to show the elastic peak used as a monitor for the absolute mass scale as well as the mass resolution. Furthermore the known elastic cross-section at 25 GeV/c[7] served as a check on the cross-section calculations in the inelastic region. The high-mass and low-mass spectra were obtained at two different settings of the turntable holding the proton telescope and were joined via the calculated cross-sections. The peak in the low-mass end of the spectra is well fitted by the mass parameters of the A_2 : M = 1.300 GeV and Γ = 100 MeV. Fitting both spectra with a polynomial background plus a Breit-Wigner resonance yields cross-sections of $d\sigma/dt$ = 177 μb/GeV^2 and 126 μb/GeV^2 [for $|\bar{t}|$ = 0.30 GeV^2] for 25 GeV/c and 40 GeV/c respectively. Thus the 1300 peak decreases with the increasing momentum by only a factor ~ 0.7. More detailed studies, including a partial wave analysis of the fitted $\pi^+\pi^-\pi^-$ system, are under way.

3. Elastic Scattering of Hadrons

Let us now take a look at the preliminary results on the elastic scattering measurements at 25 and 40 GeV/c made by this group. Figure 7 shows a comparison of the new $\pi^- p$ data with the published data of Foley et al.[7] which shows excellent agreement between the two measurements and lends confidence to the new data. The $\pi^- p$ differential cross-sections at 25 and 40 GeV/c are compared in Figure 8. Note that the data seem to fit a simple exponential form over the measured t-range of $0.09 < |t| < 0.28$ GeV^2 but that the extrapolated value of $d\sigma/dt$ in the forward direction falls well below the optical point. Figure 9 shows a similar graph for the $K^- p$ elastic scattering results. The same remark applies both for the $K^- p$ and also the $\bar{p}p$ data shown in Figure 10. The group now have in the analysis stage some four times more data on $\bar{p}p$ than is represented in Figure 10 so the slope will be better determined in the near future. Figures 11, 12 and 13 show the values of the fitted slope parameter b of these measurements compared with data obtained at lower energies and fitted in the same way over a similar $|t|$-interval.[8] Both $\pi^- p$ and $K^- p$ slopes seem to be constant but there is some indication that the $\bar{p}p$ slope is still decreasing at 40 GeV/c, although the error bars, which include statistical and systematic errors, are large at present. Note the value of b for $\bar{p}p$ scattering seems to have fallen to a level of ~ 10 GeV^{-2}.

4. Elastic Proton-Proton Scattering at the ISR

The ISR at CERN allows us to get a glimpse of phenomena at very high energies. The data I will present are all taken at one of the three following momenta for each storage ring, namely, 15.5 GeV/c, 22.7 GeV/c and 26.8 GeV/c. Table 1 shows the corresponding values of s, the square of the energy in the centre of mass and E_o, which is approximately the equivalent energy of a conventional accelerator using stationary target protons.

The first experiment to be discussed is that of the CERN-Rome collaboration.[9]. The concept of this experiment is very simple and uses 4 scintillation counter hodoscopes distributed around the interaction region as shown in Figure 14. The two conjugate pairs of hodoscopes AB and CD gave independent measurements of the elastic scattering. Each hodoscope consisted of 10 ladder counters and two trigger counters, coupled to an on-line computer. The computer classified and displayed the events as two 10 x 10 coincidence matrices (AB or CD). Each element of the matrix contained the number of coincidences in elements A_iB_j (or C_iD_j). Elastic scattering events appeared along the diagonal of a matrix since the elements A_iB_i (or C_iD_i) were collinear with the centre of the interaction region : Figure 15 shows graphically the coincidence matrix of a run at 15.5 + 15.5 GeV/c which contained 45,000 events. The prominent ridge along the diagonal reflects the characteristic angular correlation of elastic events. To extract in a simple way the t-dependence of the angular distribution, one can plot on a logarithmic scale the number of events, corrected for the small background, along the rows or columns of the matrix. Figure 15 also shows the results obtained by this technique for typical runs at the three energies studied. In the final analysis to extract the logarithmic slope b, the AB and CD matrices were fitted simultaneously taking into account the geometry of the interaction region. The values of the slope and the t-range used are shown in Table 2, and are compared with data at lower energies in Figure 16. When taken alone, with their errors, the new results cannot determine the energy dependence of b. However, if considered together with results obtained at Serpukhov [10], they lead to the conclusion that in the t-range investigated the shrinking of the forward peak

continues up to ISR energies, but less rapidly than suggested by an extrapolation of the Serpukhov data. If one compares the usual simple Regge form for b :

$$b = b_o + 2\alpha' \qquad (4)$$

and assumes $\alpha' = \frac{1}{2}$ one obtains a straight line as shown in the figure, which is in strong disagreement with the data.

Contemporaneous with the CERN-Rome experiment, another measurement of elastic proton-proton scattering was carried out by the CERN-Aachen-Torino group [11]. This experiment covered a t-range complementary to the CERN-Rome experiment in that the minimum angle measured by their spark chamber system corresponded closely with the maximum angle covered by the CERN-Rome hodoscopes. Some of their results are shown in Figure 17. The slopes obtained by this group at 22.7 and 26.8 GeV were lower than the values of the CERN-Rome group and even suggested anti-shrinking. However, one must note that their $|t|$-range was not very small and it has long been suspected [12] that there might be a change of slope in the small $|t|$-region. In order to resolve the apparent discrepancy the CERN-Aachen-Torino group modified the vacuum chamber and their spark chamber system to allow a small minimum value of $|t|$ to be reached. The results of their measurements at 22.7 GeV/c are shown in Figure 18. Indeed a distinct change of slope is seen at $|t| \approx 0.1$ GeV^2. The slope in the lower $|t|$-range is in agreement with the CERN-Rome experiment and the slope at higher $|t|$ agrees with their own earlier measurements. I note in passing that one can fit these data with the sum of two exponentials but in that case the slope of the exponential which dominates near the forward direction is about 30 GeV^{-2} ! However, other fits are also possible with equally acceptable χ^2. There is also a suggestion of a deviation just above the "break" in the distribution of Figure 18, but this is possibly a statistical fluctuation, although it seems unlikely.

The group are now analyzing similar data taken at other energies which should shed further light on these phenomena.

5. Particle Production at the ISR

Two experiments at the ISR on particle production have produced results already. The first one has been carried out by the Argonne-Bologna-Michigan collaboration and has studied the production of positively charged secondaries at relatively large angles. Preliminary results have already appeared in the literature [13] and a report was presented at the APS Rochester Conference in August of this year [14], so I will only present the results and briefly discuss them.

The results are presented in Figure 19 in the form of an invariant cross-section $E\, d^2\sigma/dP^3$ $(= \frac{E}{P^2} \cdot \frac{d^2\sigma}{d\Omega dP})$ for data taken at fixed values of $P_\perp$ plotted against the scaling variable $X = P_{\parallel}/P_{max}$, where P_{max} is the maximum value of $P_{\parallel}$. The data show that the particle production cross-sections plotted in this way are independent of the incident proton momentum within the experimental errors and for X less than 0.5. Fig. 20 shows the same data plotted against $P_\perp^2$. The authors point out the striking difference between π^+ production and proton production at small values of $P_\perp$. Yen and Berger [15] have attributed this sharpening-up of the π^+ distribution as due to the contribution from the decay of low mass nucleon isobars.

Another experiment has recently produced results on the production of γ-rays in p-p interactions [16]. The γ-rays were detected by a Pb converter followed by a Lucite Cerenkov counter to detect the electron-positron pair, and a Pb-glass total absorption counter which measured the γ-ray energy. In order to reduce background a trigger was used which demanded that a beam-beam interaction had taken place. This consisted of large scintillation counters around the beam-pipe downstream of the interaction region. A beam-beam interaction is signalled by one or more particles through each of the two beam-beam counters. (One around the vacuum chamber of ring 1, the other around the vacuum chamber of ring 2.) The efficiency of this beam-beam trigger was about 50% and the group studied the effects of reducing this efficiency by as much a factor of ten, on their spectra of γ-rays. They claim that this

trigger does not introduce any bias in the results.

The energy spectra of γ-rays produced at 90° are shown in Figure 21 together with data at a centre-of-mass energy of 6.7 GeV obtained some years ago at the CPS[17]. A single exponential

$$\frac{dN}{dK} = c.e^{-K/K_o} \qquad (5)$$

gives an excellent fit to the data. The average momentum K_o is determined by the fit and the results are shown in Table 3. Clearly the value of K_o is independent of energy from 6.7 GeV up to 53 GeV.

The main source of γ-rays is π^o-decay. It can be shown [18] that the transverse momentum distribution of π^o (at 90°) is given by the derivative of the γ-ray spectrum,

$$\frac{dN(\pi^o)}{dp_\perp^2} = \frac{-1}{4}\frac{d}{dK}\left[\frac{dN(\gamma)}{dK}\right]\Bigg|_{K = p_\perp} \qquad (6)$$

provided $p_\perp \gg m_{\pi/2}$. Thus one concludes that the average transverse momentum of the π^o at 90° is $\langle p_\perp \rangle = 2K_o$.

By integrating the spectra of Figure 21, one can obtain the value of $(d\sigma/d\Omega)$ for production of γ-rays at 90° which is shown in Table 3 and in Figure 22. The cross-section appears to have reached an asymptotic value at ISR energies.

6. Conclusion

In line with the aim of the organisers of this Conference, I have tried to present new experimental results in the field of High Energy Strong Interactions. Many of these results present problems of interpretation.

Although there seem to be many ways of fitting the new total cross-section data obtained at the Serpukhov accelerator, usually by the introduction of Regge-cuts, a detailed understanding is lacking. The success of the simple Regge-Model at lower energies seems to continue when one considers only the cross-section differences between particle and antiparticle, but the major part of the cross-sections, which is attributed to Pomeron exchange and higher order terms seems to be still only partially understood.

The new data on the spectrum of bosons at high energies shows a qualitative difference compared with lower energies. Why is the A_2 meson so preferentially produced, whilst many other possible resonances have disappeared into the continuum ?

The proton-proton elastic scattering at the ISR has yielded a new feature in the angular distribution at very small momentum transfers. Is this yet another manifestation of Regge-cuts or is there a more direct and perhaps more exciting interpretation ?

Thus I conclude by underlining some questions raised by the new data and hope that my theoretical colleagues will perhaps suggest some answers.

Table 1

Centre of mass energy squared (s) and effective energy for the three conditions of ISR operation for which data exist.

Momenta of ISR beams (GeV/c)	s GeV^2	E_o (Effective) GeV
15.5 + 15.5	930	500
22.7 + 22.7	2000	1060
26.8 + 26.8	2800	1500

Table 2

Values of the logarithmic slope b obtained for p-p elastic scattering by the CERN-Rome Group [9].

Momenta of ISR beams (GeV/c)	t range (GeV^2)	Slope parameter b (GeV^{-2})
15.5 + 15.5	0.015 - 0.055	13.0 ± 0.7
22.7 + 22.7	0.03 - 0.12	12.9 ± 0.4
26.8 + 26.8	0.04 - 0.16	13.0 ± 0.3

Table 3

Results of the ISR experiment [16] on the spectrum of γ-rays at 90^o

c.m. energy s (GeV)	Slope parameter K_o (MeV)	Flux density at 90^o $(1/\sigma_{inel})$ $(d\sigma/d\Omega)$ (sr^{-1})
6.7	152 + 10	0.15 + 0.02
30.2	167 + 8	0.22 + 0.02
44.7	161 + 9	0.23 + 0.02
52.7	161 + 8	0.24 + 0.02

References

1) J.V. Allaby, Yu. B. Bushnin, Yu. P. Gorin, S.P. Denisov, G. Giacomelli, A.N. Diddens, R.W. Dobinson, S.V. Donskov, A. Klovning, A.I. Petrukhin, Yu. D. Prokoshkin, C.A. Stahlbrandt, D.A. Stoyanova and R.S. Shuvalov, Phys. Lett. 30B, 500 (1969); Yadernaya Fizika 12, 538 (1970).

2) S.P. Denisov, Yu. P. Dmitrevski, S.B. Donskov, Yu. P. Gorin, Au.M. Melnik, A.I. Petrukhin, Yu. D. Prokoshkin, V.S. Seleznev, R.S. Shuvalov, D.A. Stoyanova and L.M. Vasiljev, Phys. Lett. 36B, 528 (1971).

3) S.P. Denisov, S.V. Donskov, Yu.P.Gorin, A.I.Petrukhin, Yu.D.Prokoshkin, D.A. Stoyanova, J.B. Allaby and G. Giacomelli, Phys. Lett. 36B, 415 (1971).

4) K.J. Foley, R.S. Jones, S.J. Lindenbaum, W.A. Love, S. Ozaki, E.D.Platner, C.A. Quarles and E.H. Willen, Phys. Rev. Lett. 19, 330 (1967) and Phys. Rev. Lett. 19, 857 (1967).

5) H.J. Lipkin, "Omega Universality Revisited", preprint 1971.

6) The author would like to thank W. Kienzle and P. Martin of the CERN Boson Spectrometer Group for communicating these results prior to publication.

7) K.J. Foley, R.S. Jones, S.J. Lindenbaum, W.A. Love, S. Ozaki, E.D. Platner, C.A. Quarles and E.H. Willen, Phys. Rev. 181, 1775 (1969).

8) T. Lasinski, R. Levi-Setti, B. Schwarzschild and P. Ukleja, "Redetermination of diffraction slopes in meson-baryon and baryon-baryon scattering", University of Chicago, Report EFI 70-50 (1970).

9) U. Amaldi, R. Biancastelli, C. Bosio, G. Matthiae, J.V. Allaby, W. Bartel, G. Cocconi, A.N. Diddens, R.W. Dobinson, V. Elings, J. Litt, L.S.Rochester and A.M. Wetherell, Phys. Lett. 36 B, 504 (1971).

10) G.G. Beznogikh, A. Bucjak, K.I. Iovchev, L.F. Kirillova, P.K. Markov, B.A. Morozov, V.A. Nikitin, P.V. Nomokonov, M.G. Stafranova, V.A. Sviridov, Truong Bien, V.I. Zayachki, N.K. Zhidkov, L.S. Zolin, S.B. Nurushev and V.L. Solovianov, Phys. Lett. 30 B, 275 (1969).

11) M. Holder, E. Radermacher, A. Staude, G. Barbiellini, P. Darriulat, M. Hansroul, S. Orito, P. Palazzi, A. Santroni, P. Strolin, K. Tittel, J. Pilcher, C. Rubbia, G. de Zorzi, M. Macri, G. Sette, C. Grosso-Pilcher, A. Fainberg and G. Maderni, Phys. Lett. 35 B, 355 (1971).

12) R.A. Carrigan, Phys. Rev. Lett. 24, 168 (1970).

13) L.G. Ratner, R.J. Ellis, G. Vannini, B.A. Babcock, A.D. Krisch and J.B. Roberts, Phys. Rev. Lett. 27, 68 (1971).

14) L.G. Ratner, R.J. Ellis, G. Vannini, B.A. Babcock, A.D. Krisch and J.B. Roberts, "Inelastic Proton-Proton Scattering at Very High Energy", presented at the Rochester Conference on High Energy Physics, 31 Aug. 1971.

15) E Yen and E. Berger, Phys. Rev. Lett. 24, 695 (1970).

16) G. Neuhofer, F. Niebergall, J. Penzias, M. Regler, K.R. Schubert, P.E. Schumacher, W. Schmidt-Parzefall and K. Winter, Phys.Lett. 37B, 438 (1971).

17) M. Fidecaro, G. Finocchiaro, G. Gatti, G. Giacomelli, W.C. Middelkoop and T. Yamagata, Nuovo Cimento 24, 73 (1962).

18) R.M. Sternheimer, Phys. Rev. 99, 277 (1955).

Figure Captions

Fig. 1 : Compilation of particle and antiparticle total cross-sections on liquid hydrogen, as a function of incident momentum.

Fig. 2 : Differences between particle and antiparticle total cross-sections as a function of incident momentum. The solid lines are least-squared fits to the data shown.

Fig. 3 : Plot of the expression $\Delta = 3\left[\sigma_t(K^-d) - \sigma_t(K^+d)\right] - \left[\sigma_t(\bar{p}d) - \sigma_t(pd)\right]$, as a function of incident momentum. The error bars are statistical errors only. The effect of systematic scale errors is represented by the shaded region.

Fig. 4 : Diagram of the experimental equipment used by the CERN-IHEP group in their measurements on boson production at high energies.

Fig. 5 : Boson mass-spectrum obtained at CERN in various low energy experiments.

Fig. 6 : Mass spectrum obtained at 25 and 40 GeV/c by the CERN-IHEP collaboration. The double differential cross-section $d^2\sigma/dtdM^2$ is shown plotted against $M(X)^2$.

Fig. 7 : Comparison between the π^-p elastic scattering data obtained at Serpukhov and the published data of Foley et al. [7].

Fig. 8 : Differential cross-sections for π^-p elastic scattering.

Fig. 9 : Differential cross-section for K^-p elastic scattering.

Fig. 10 : Differential cross-sections for $\bar{p}p$ elastic scattering.

Fig. 11 : Values of the exponential slope b for π^-p elastic scattering.

Fig. 12 : Values of the exponential slope b for K^-p elastic scattering.

Fig. 13 : Values of the exponential slope b for $\bar{p}p$ elastic scattering.

Fig. 14 : Diagram of experimental equipment at the ISR used by the CERN-Rome group in their measurements of proton-proton elastic scattering.

Fig. 15 : Typical data obtained by the CERN-Rome group on elastic proton-proton scattering, using conjugate hodoscopes of scintillation counters. The prominent ridge along the diagonal of the AB matrix reflects the characteristic angular correlation of elastic events. The angular distributions obtained at three ISR momenta shown on the right of the figure are obtained by projecting the data onto either the A or the B axis.

Fig. 16 : Compilation of values of the slope parameter b for elastic proton-proton scattering at small angles, as a function of s.

Fig. 17 : Typical data obtained by the CERN-Aachen-Torino group [11], using wire spark chambers to detect both scattered protons.

Fig. 18 : Data taken by the CERN-Aachen-Torino group after extending their measurements to smaller angles.

Fig. 19 : Data on particle production obtained by the Argonne-Bologna-Michigan collaboration at the ISR [14], plotted against the scaling variable X.

Fig. 20 : The same data as Fig. 19 but plotted against $P_\perp^2$.

Fig. 21 : Spectra of γ-rays produced at 90° in the centre of mass system at the ISR obtained by the CERN-Hamburg-Vienna group [16], compared with lower energy data [17].

Fig. 22 : Integrated cross-section for γ-ray production at 90° plotted against $\sqrt{s}$.

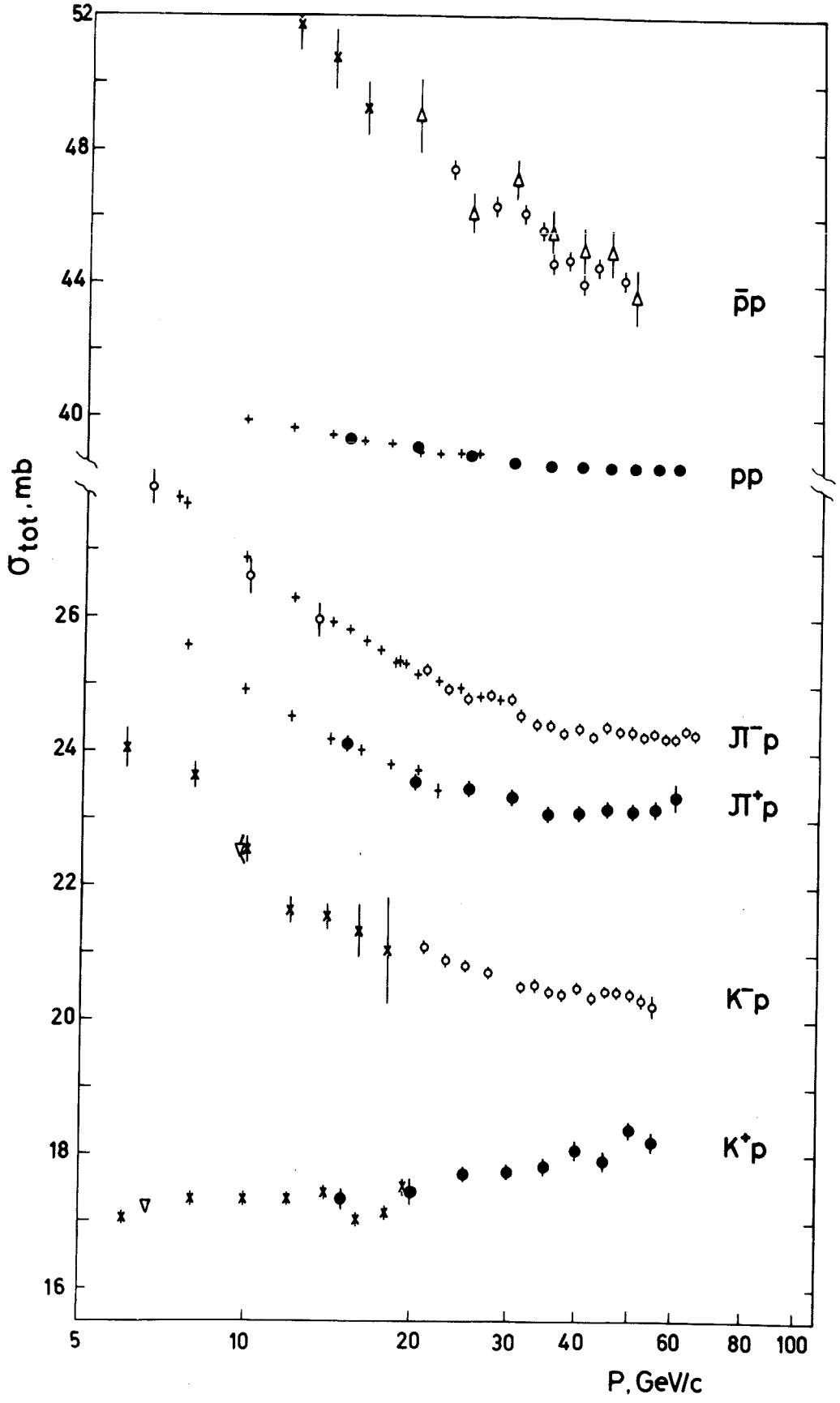
52
48
44
40
26
24
22
20
18
16
σ_{tot}, mb
$\bar{p}p$
pp
π^-p
π^+p
K^-p
K^+p
5
10
20
30
40
60
80
100
P, GeV/c

Fig. 1

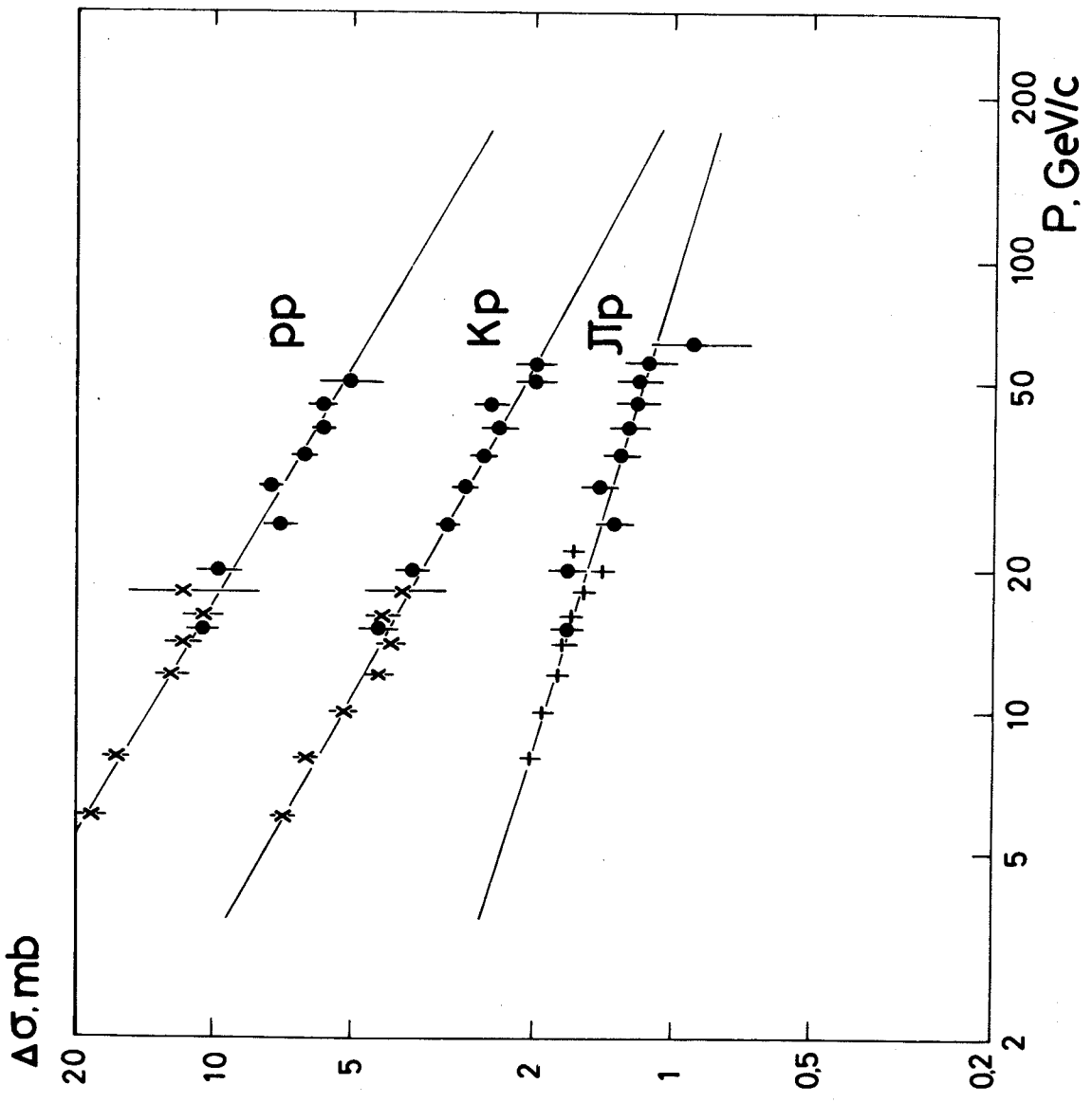

Fig. 2

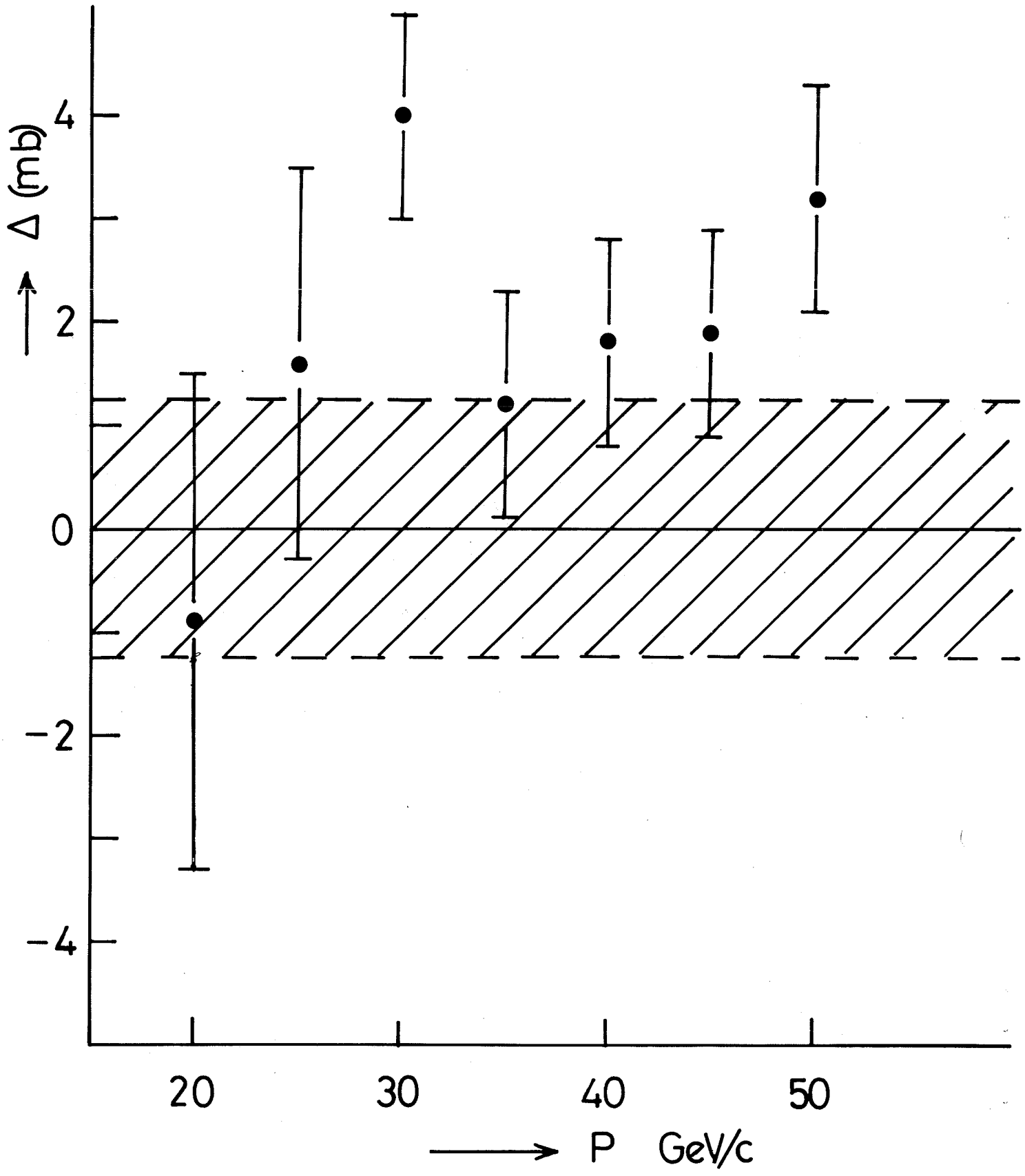

Fig. 3

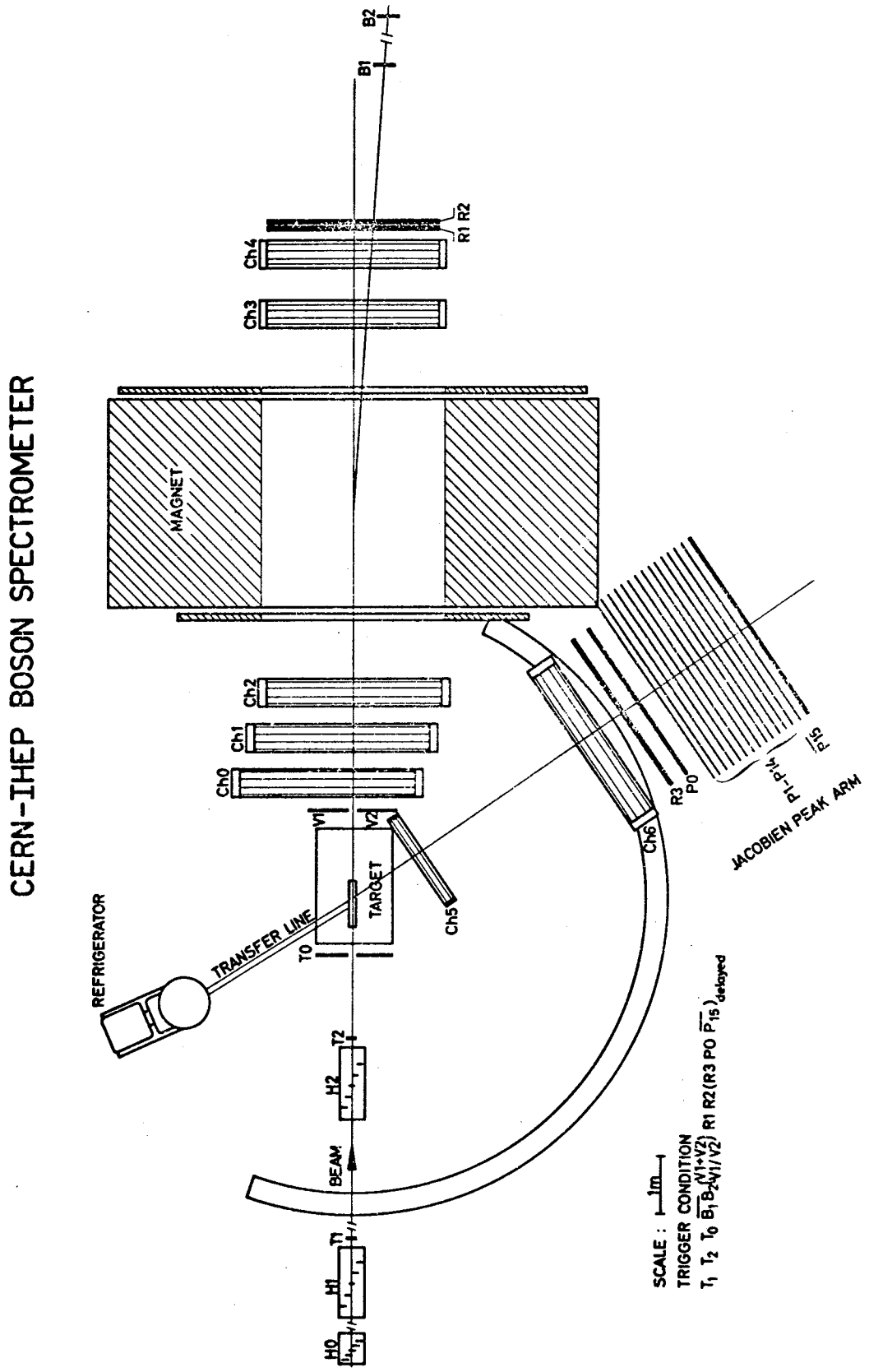
CERN-IHEP BOSON SPECTROMETER
B2
B1
R1 R2
Ch4
Ch3
MAGNET
Ch2
Ch1
Ch0
V1
V2
TARGET
Ch5
Ch6
R3
P0
P1-P4
P5
JACOBIEN PEAK ARM
REFRIGERATOR
TRANSFER LINE
T0
T2
H2
BEAM
T1
H1
H0
SCALE : 1m
TRIGGER CONDITION
T1 T2 T0 B1 B2 (V1+V2) R1 R2 (R3 P0 P15)delayed

Fig. 4

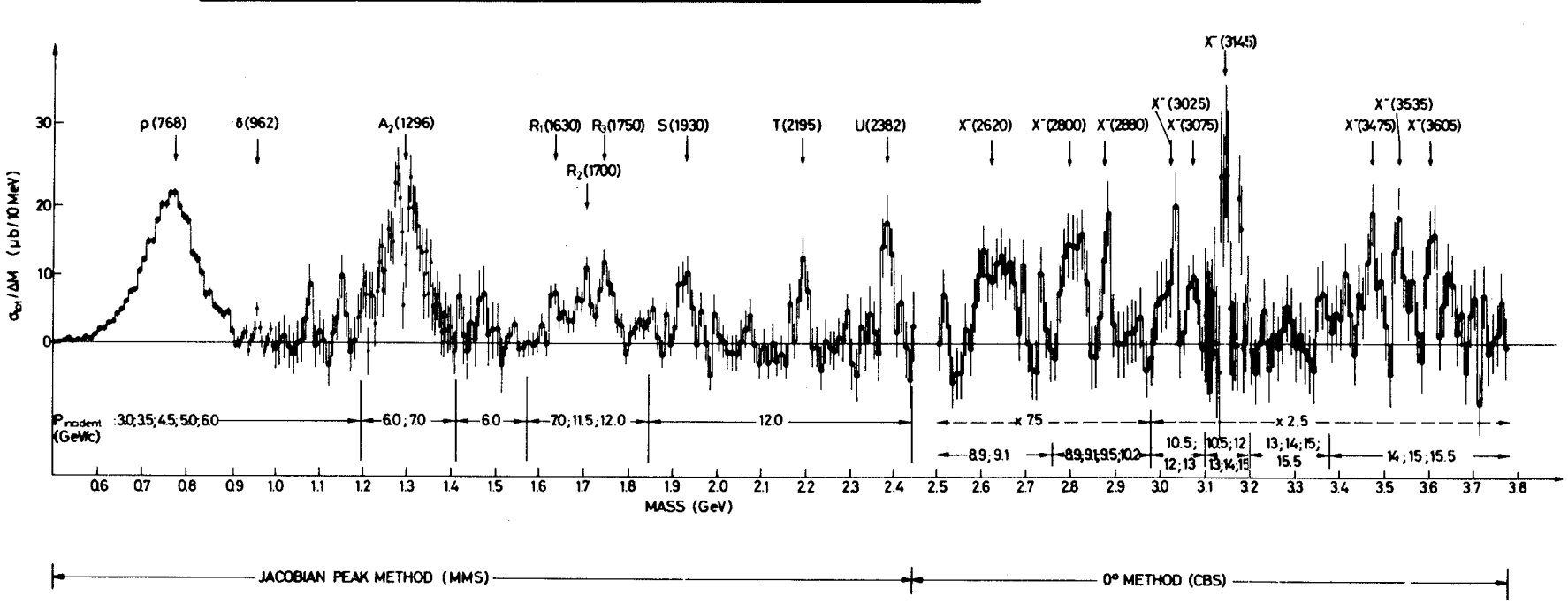
BOSON MASS-SPECTRUM IN π⁻+p → p+(BOSON)⁻, CERN 1965-70
ρ(768)
δ(962)
A₂(1296)
R₁(1630)
R₃(1750)
R₂(1700)
S(1930)
T(2195)
U(2382)
X⁻(2620)
X⁻(2800)
X⁻(2880)
X⁻(3025)
X⁻(3075)
X⁻(3145)
X⁻(3475)
X⁻(3535)
X⁻(3605)
dσ/ΔM (μb/10MeV)
P incident (GeV/c)
30;35;45;50;60
60;70
60
70;115;120
120
x 7.5
x 2.5
89;91
89;91;95;102
105;12
105;12
13;14;15;
15.5
14;15;15.5
MASS (GeV)
JACOBIAN PEAK METHOD (MMS)
0° METHOD (CBS)

Fig. 5

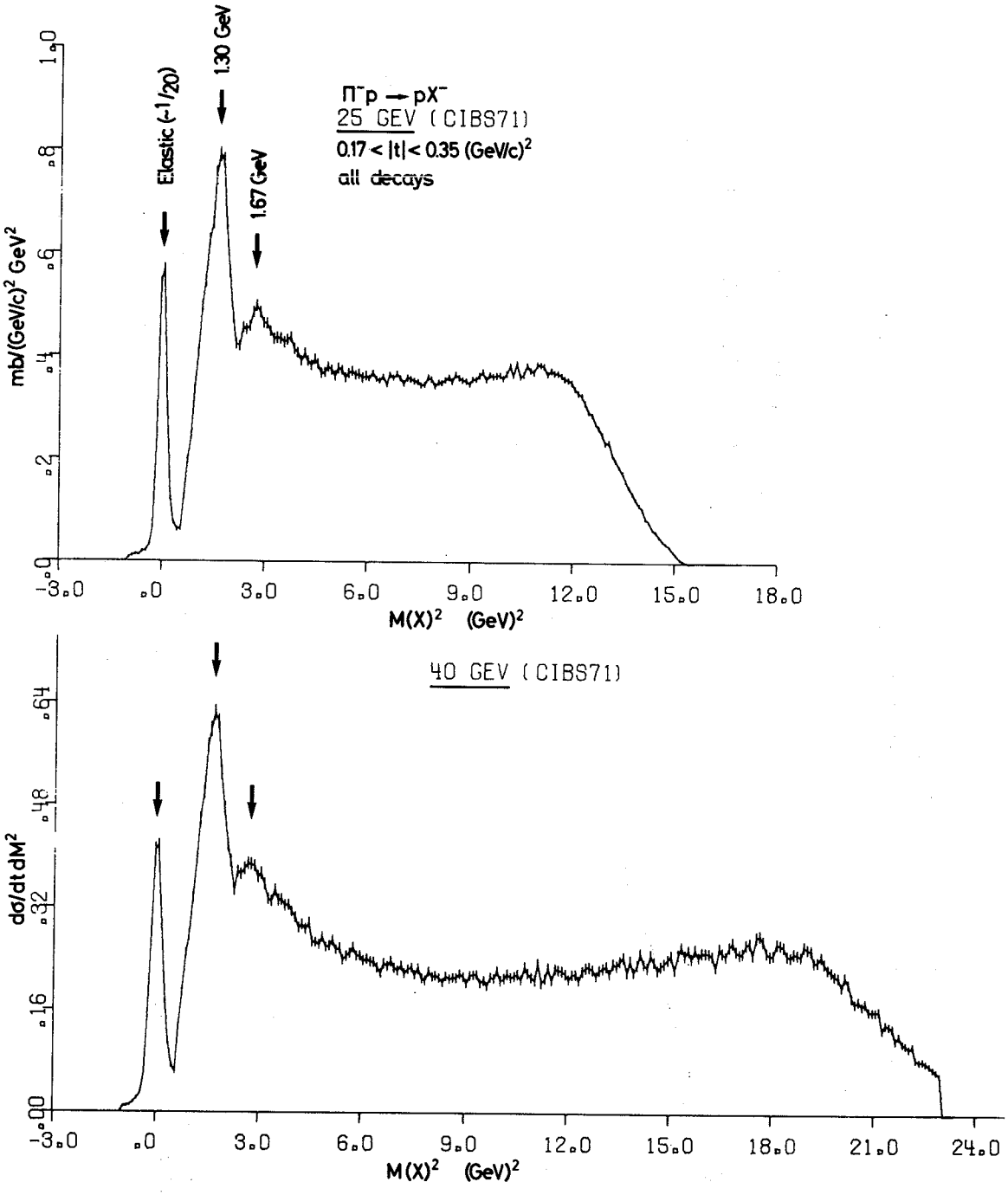
Elastic (~1/20)
1.30 GeV
1.67 GeV
π⁻p → pX⁻
25 GEV (CIBS71)
0.17 < |t| < 0.35 (GeV/c)²
all decays
mb/(GeV/c)² GeV²
M(X)² (GeV)²
40 GEV (CIBS71)
dσ/dt dM²
M(X)² (GeV)²

Fig. 6

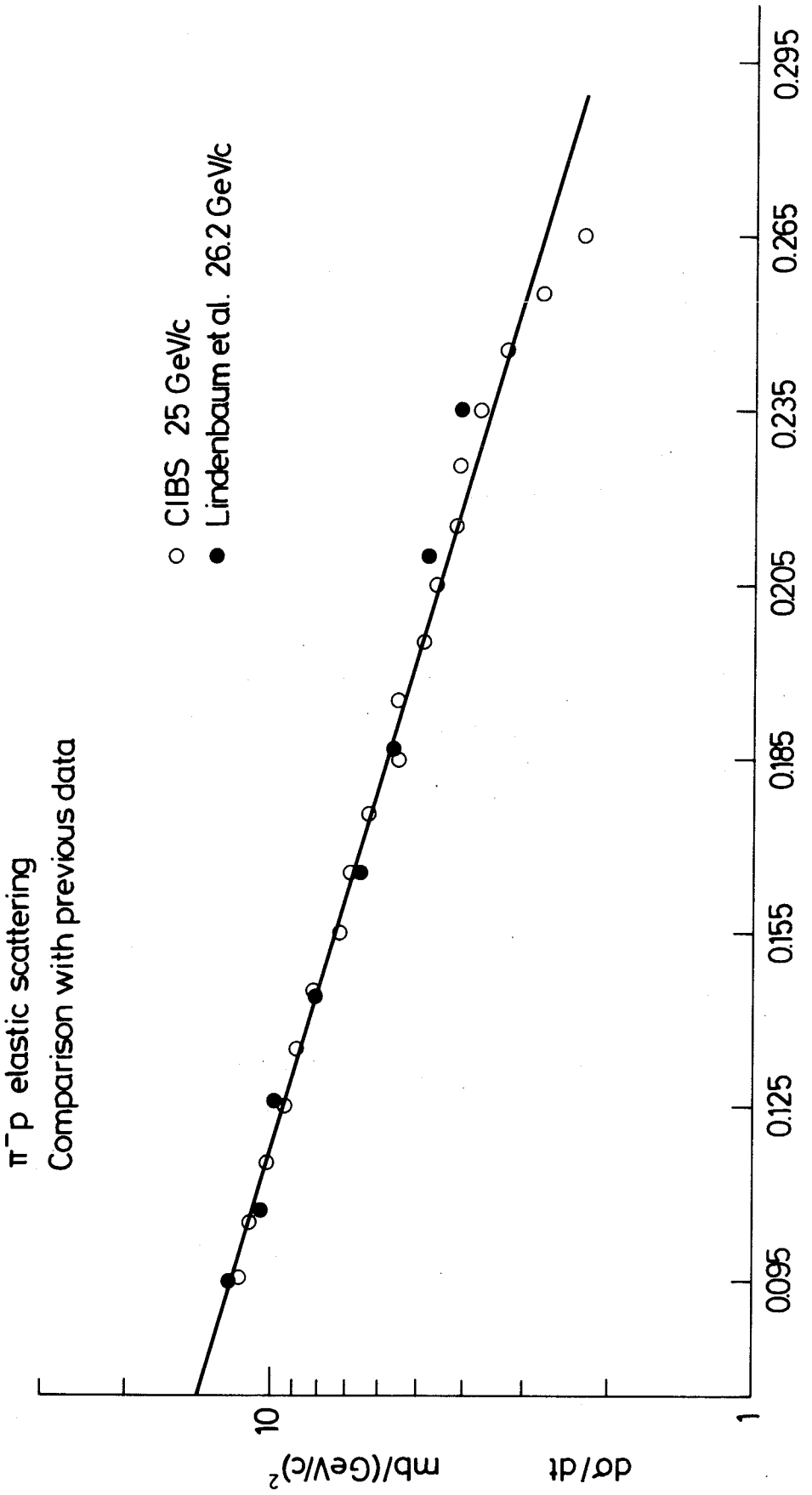
π⁻p elastic scattering
Comparison with previous data
○ CIBS 25 GeV/c
● Lindenbaum et al. 26.2 GeV/c
dσ/dt
mb/(GeV/c)²
10
1
0.095
0.125
0.155
0.185
0.205
0.235
0.265
0.295
t (GeV/c)²

Fig. 7

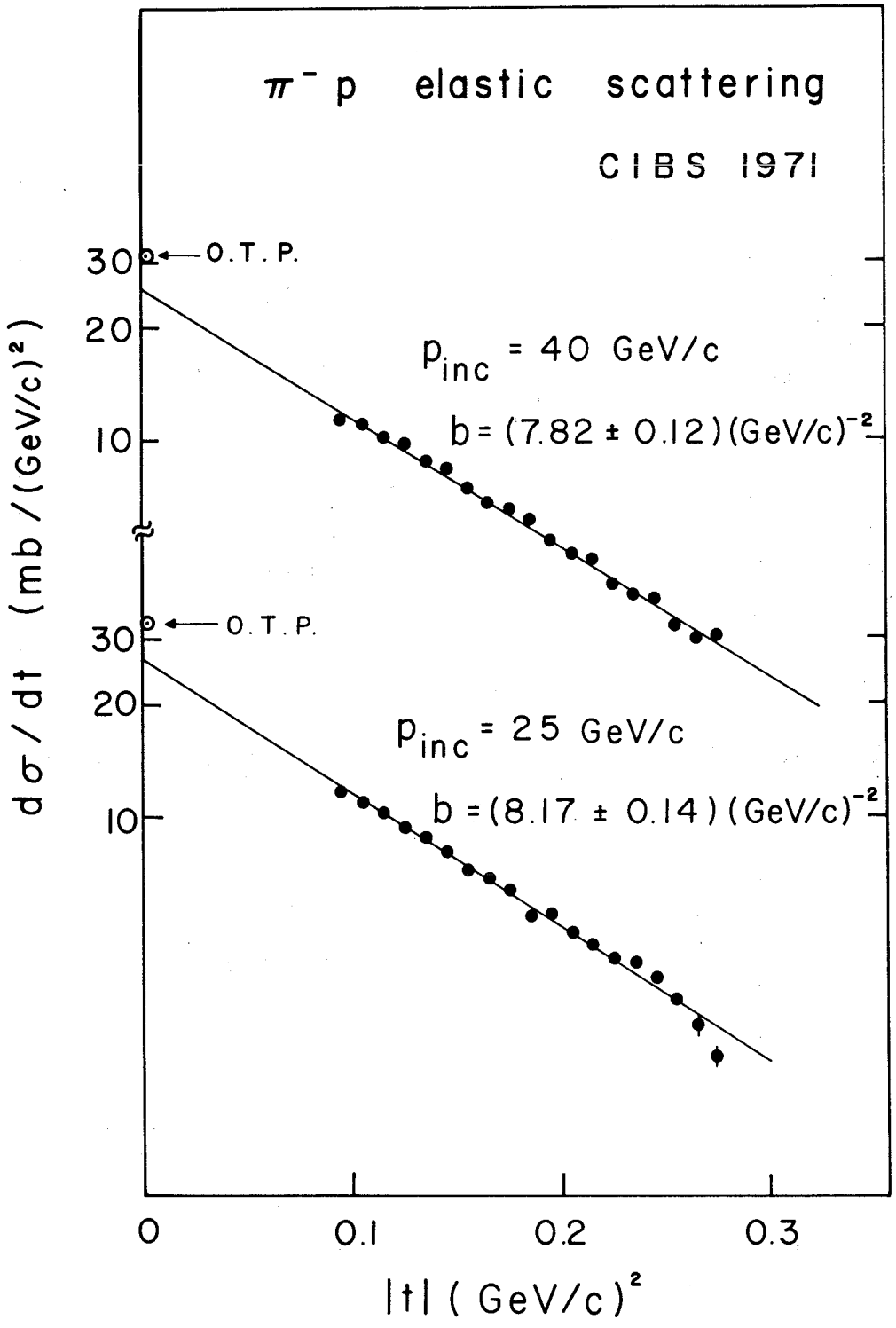
π⁻ p elastic scattering
CIBS 1971
O.T.P.
30
20
10
p_{inc} = 40 GeV/c
b = (7.82 ± 0.12) (GeV/c)⁻²
O.T.P.
30
20
10
p_{inc} = 25 GeV/c
b = (8.17 ± 0.14) (GeV/c)⁻²
dσ/dt (mb/(GeV/c)²)
0
0.1
0.2
0.3
|t| (GeV/c)²

Fig. 8

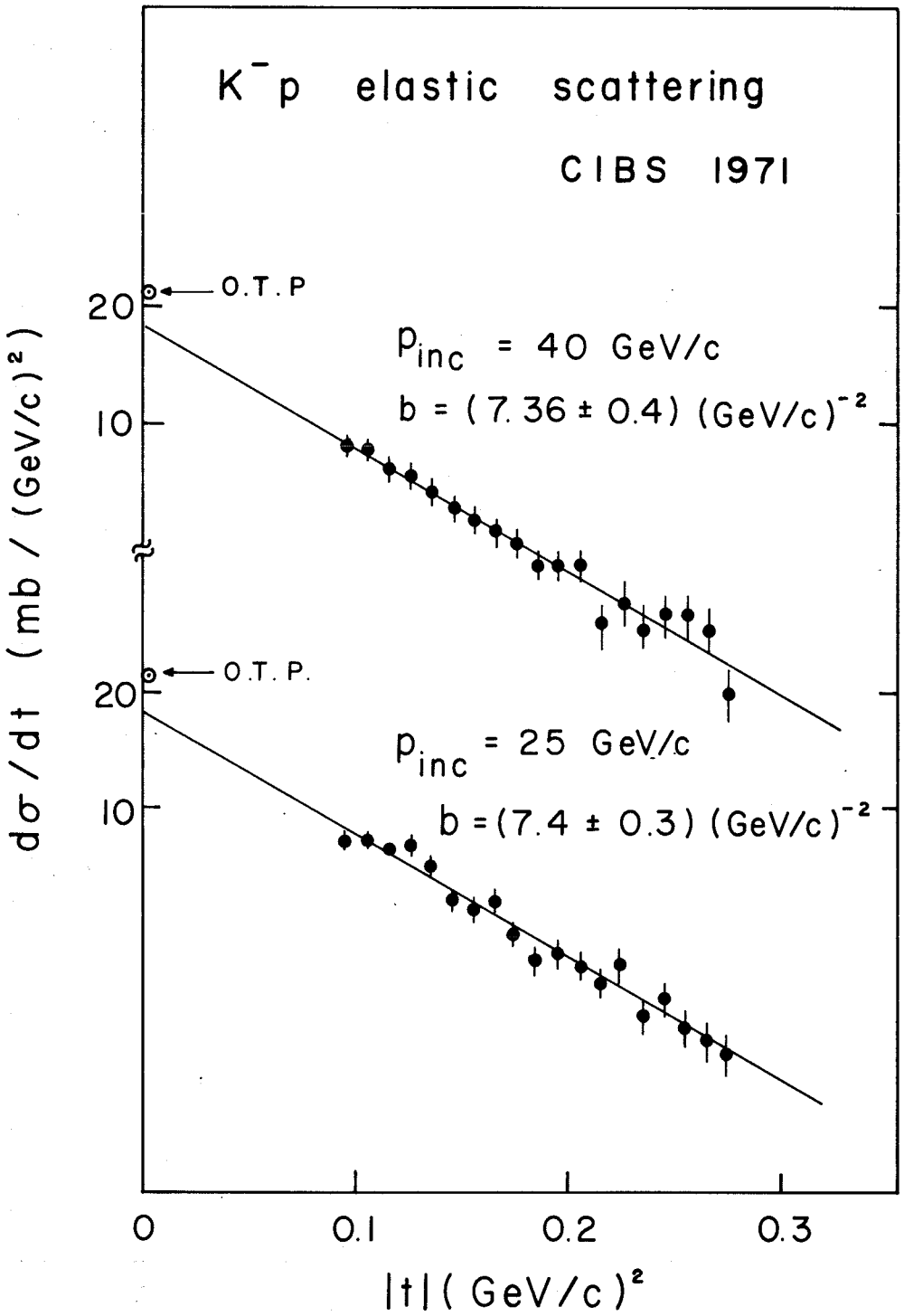
K⁻p elastic scattering
CIBS 1971
O.T.P
20
10
p_{inc} = 40 GeV/c
b = (7.36 ± 0.4) (GeV/c)$^{-2}$
O.T.P.
20
10
p_{inc} = 25 GeV/c
b = (7.4 ± 0.3) (GeV/c)$^{-2}$
dσ/dt (mb / (GeV/c)²)
0
0.1
0.2
0.3
|t| (GeV/c)²

Fig. 9

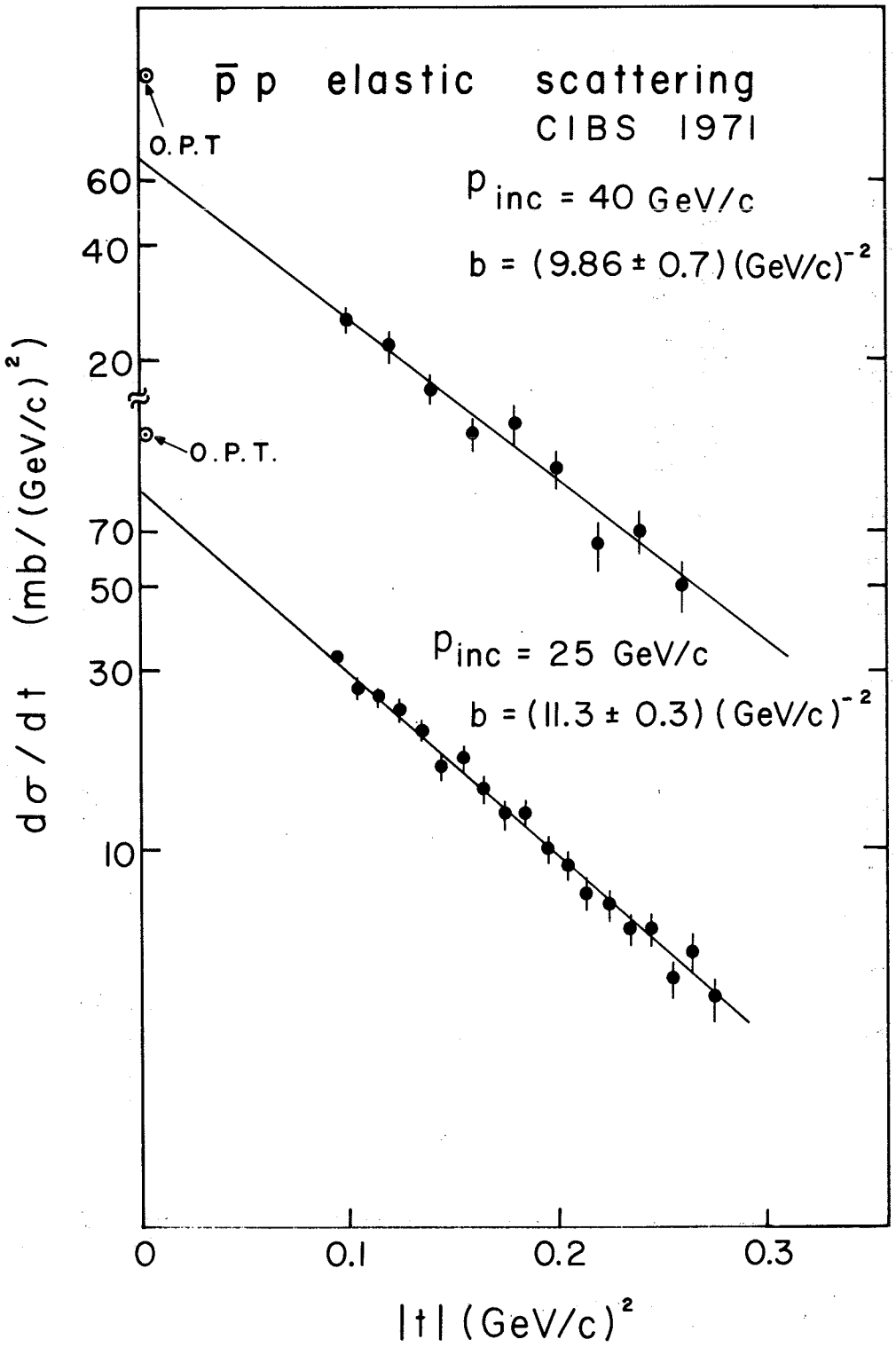
p̄ p elastic scattering
CIBS 1971
O.P.T
O.P.T.
p inc = 40 GeV/c
b = (9.86 ± 0.7) (GeV/c)⁻²
p inc = 25 GeV/c
b = (11.3 ± 0.3) (GeV/c)⁻²
dσ/dt (mb/(GeV/c)²)
60
40
20
70
50
30
10
0
0.1
0.2
0.3
|t| (GeV/c)²

Fig. 10

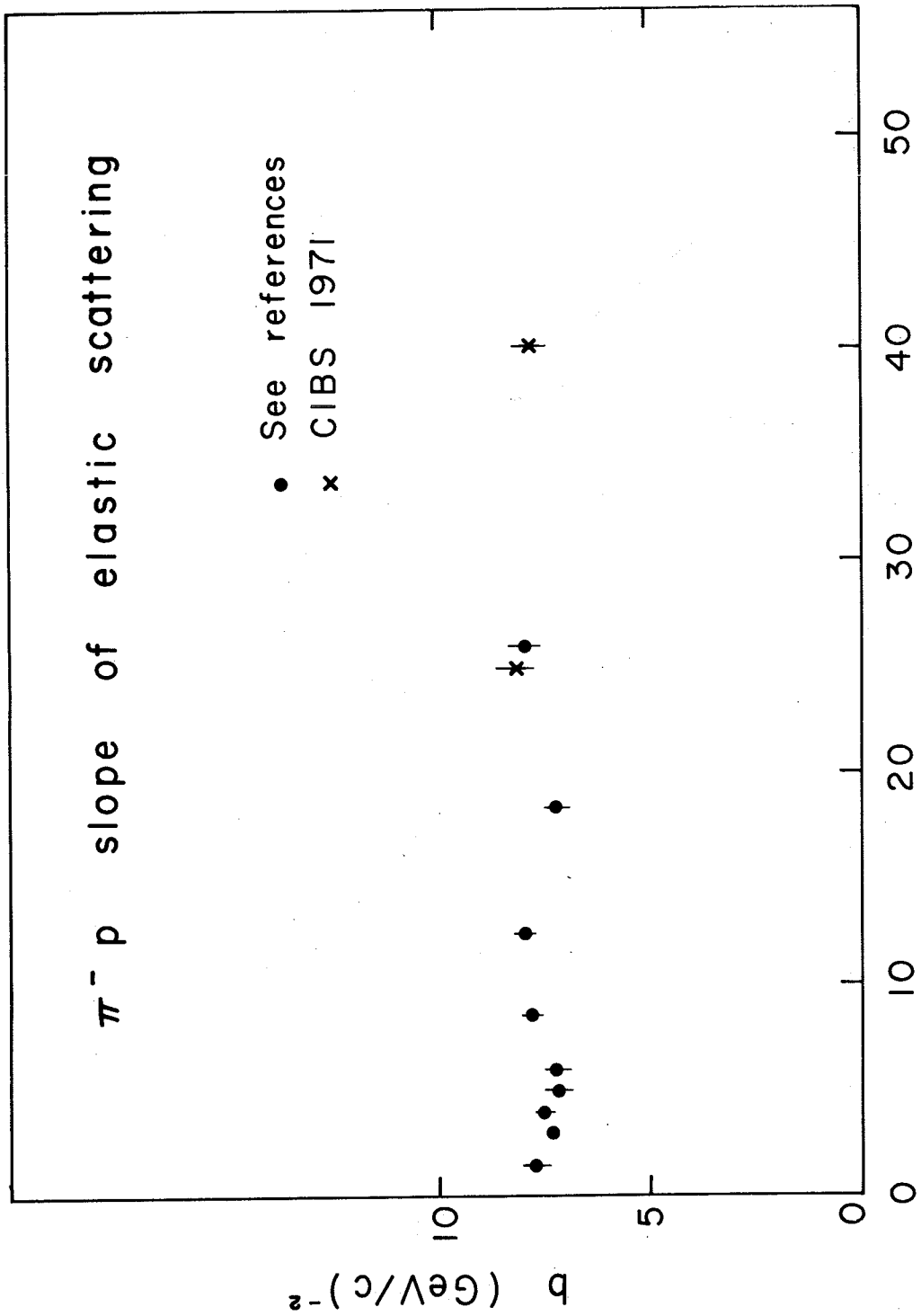
π^- p slope of elastic scattering
See references
CIBS 1971
b (GeV/c)$^{-2}$
p_{inc} (GeV/c)
0
5
10
0
10
20
30
40
50

Fig. 11

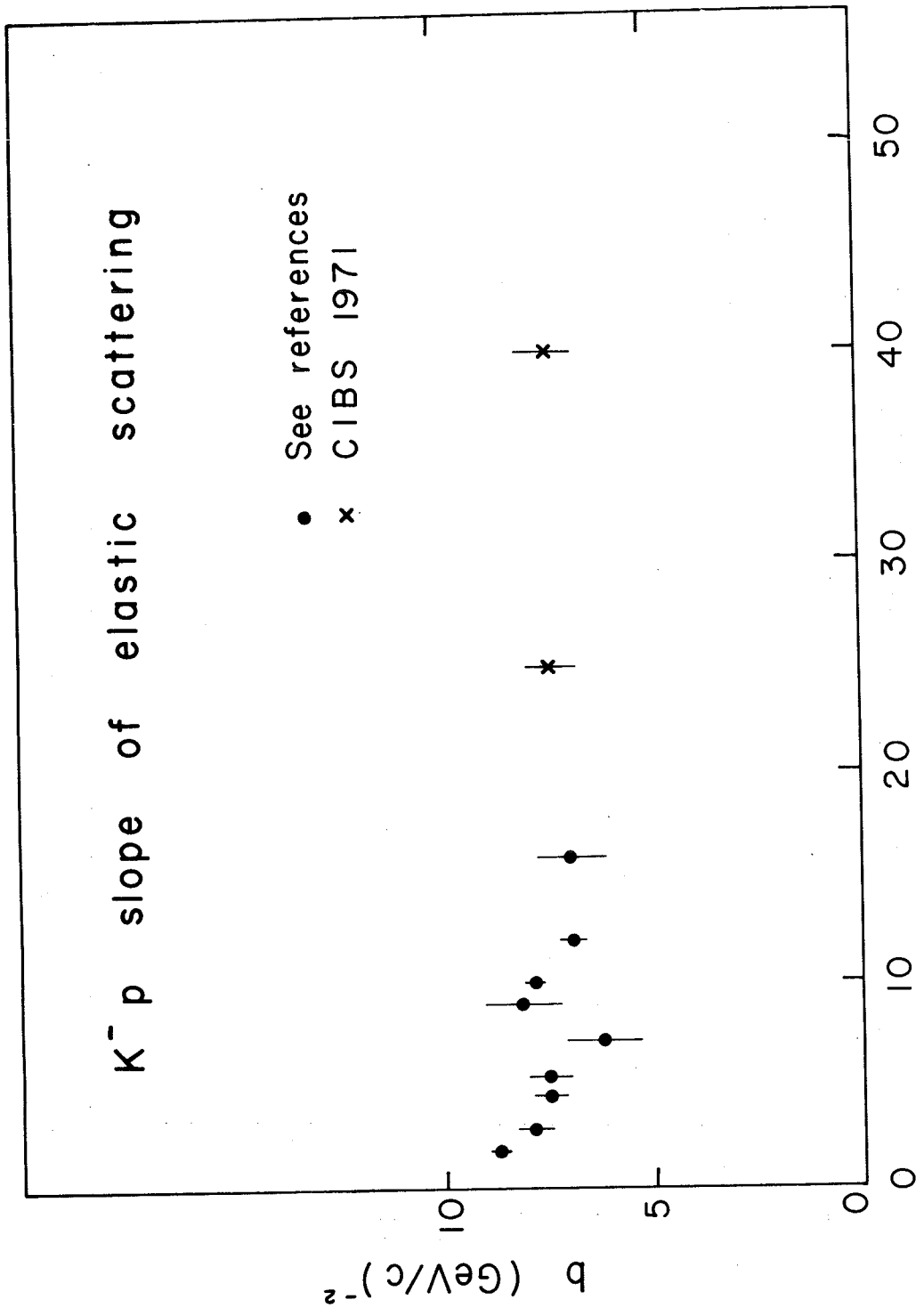
K⁻p slope of elastic scattering
See references
CIBS 1971
b (GeV/c)⁻²
10
5
0
0
10
20
30
40
50
p_inc (GeV/c)

Fig. 12

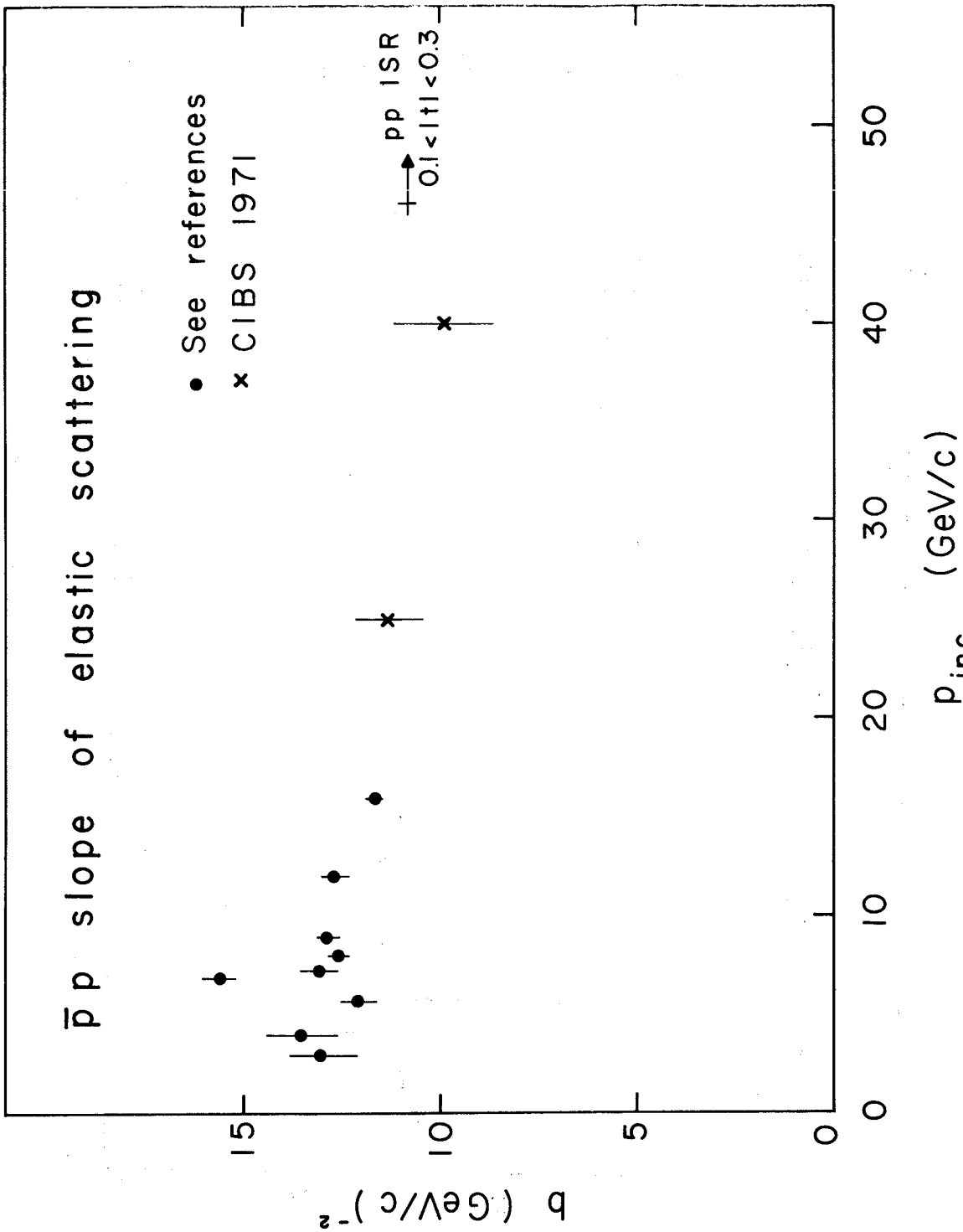
$\bar{p}p$ slope of elastic scattering
• See references
× CIBS 1971
pp ISR
0.1<|t|<0.3
b (GeV/c)$^{-2}$
p_{inc} (GeV/c)
0
5
10
15
0
10
20
30
40
50

Fig. 13

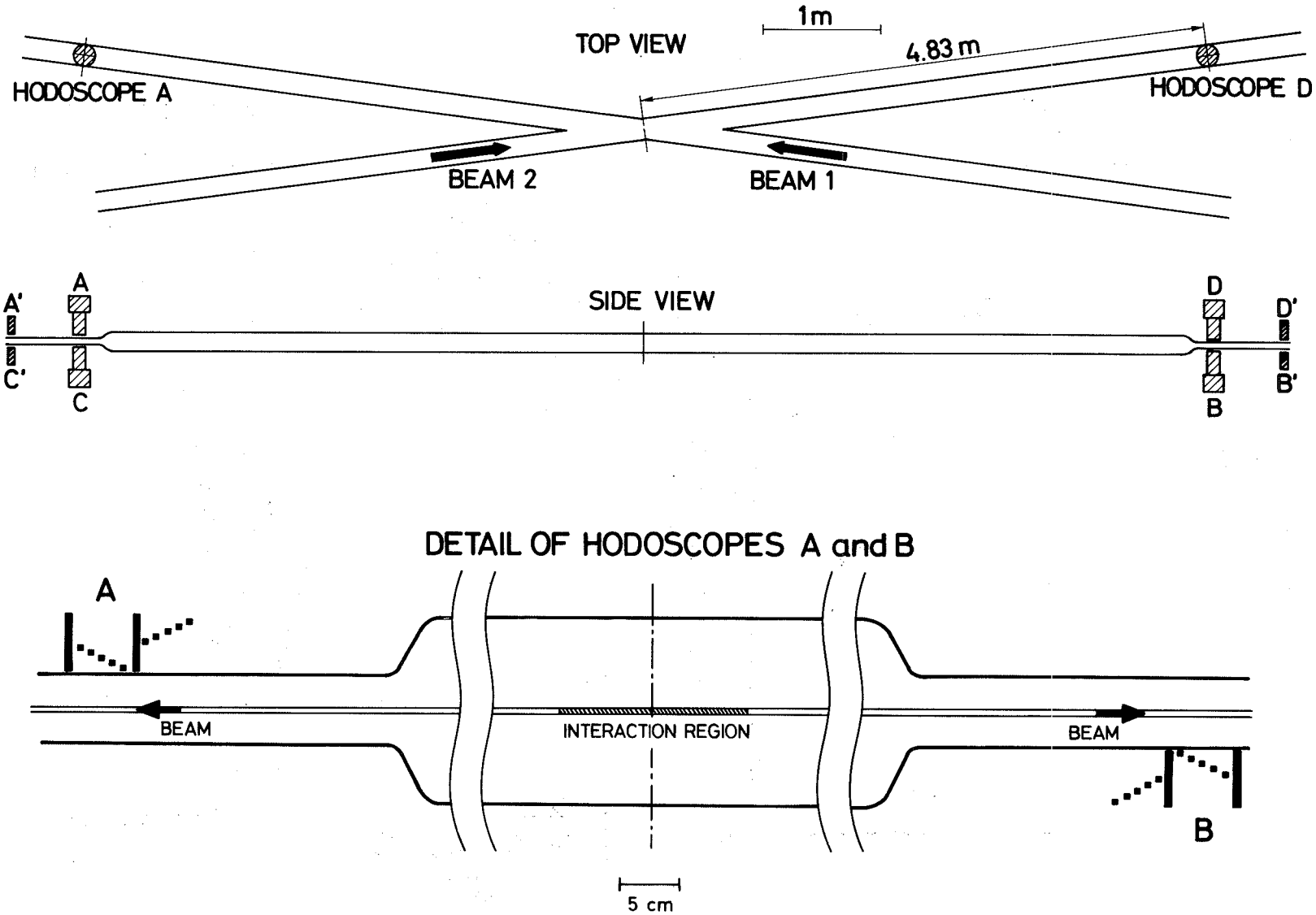
TOP VIEW
1m
4.83 m
HODOSCOPE A
HODOSCOPE D
BEAM 2
BEAM 1
SIDE VIEW
A'
A
C'
C
D
D'
B
B'
DETAIL OF HODOSCOPES A and B
A
BEAM
INTERACTION REGION
BEAM
B
5 cm

Fig. 14

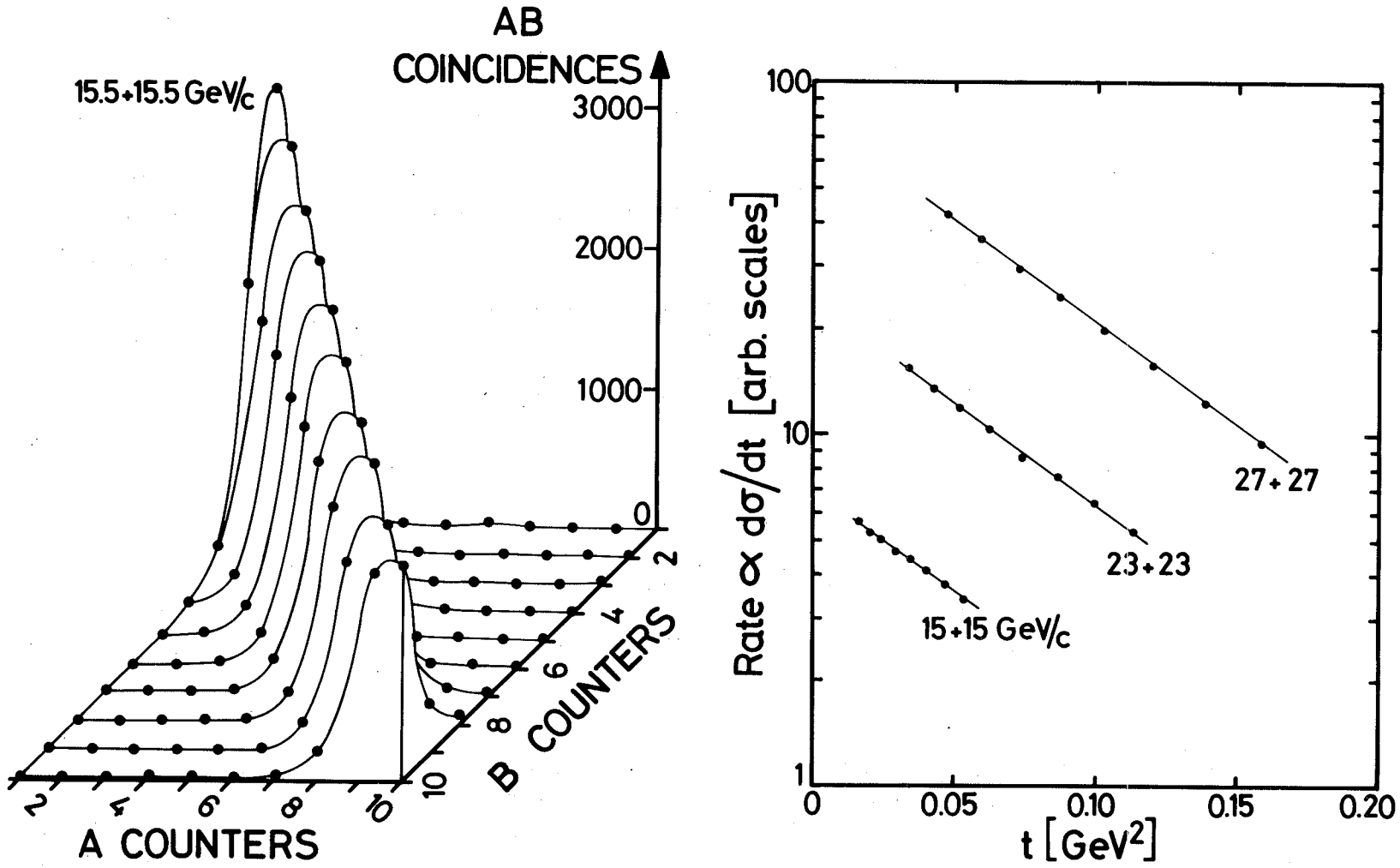
AB
COINCIDENCES
15.5+15.5 GeV/c
3000
2000
1000
0
A COUNTERS
B COUNTERS
Rate ∝ dσ/dt [arb. scales]
100
10
1
0
0.05
0.10
0.15
0.20
t [GeV²]
27+27
23+23
15+15 GeV/c

Fig. 15

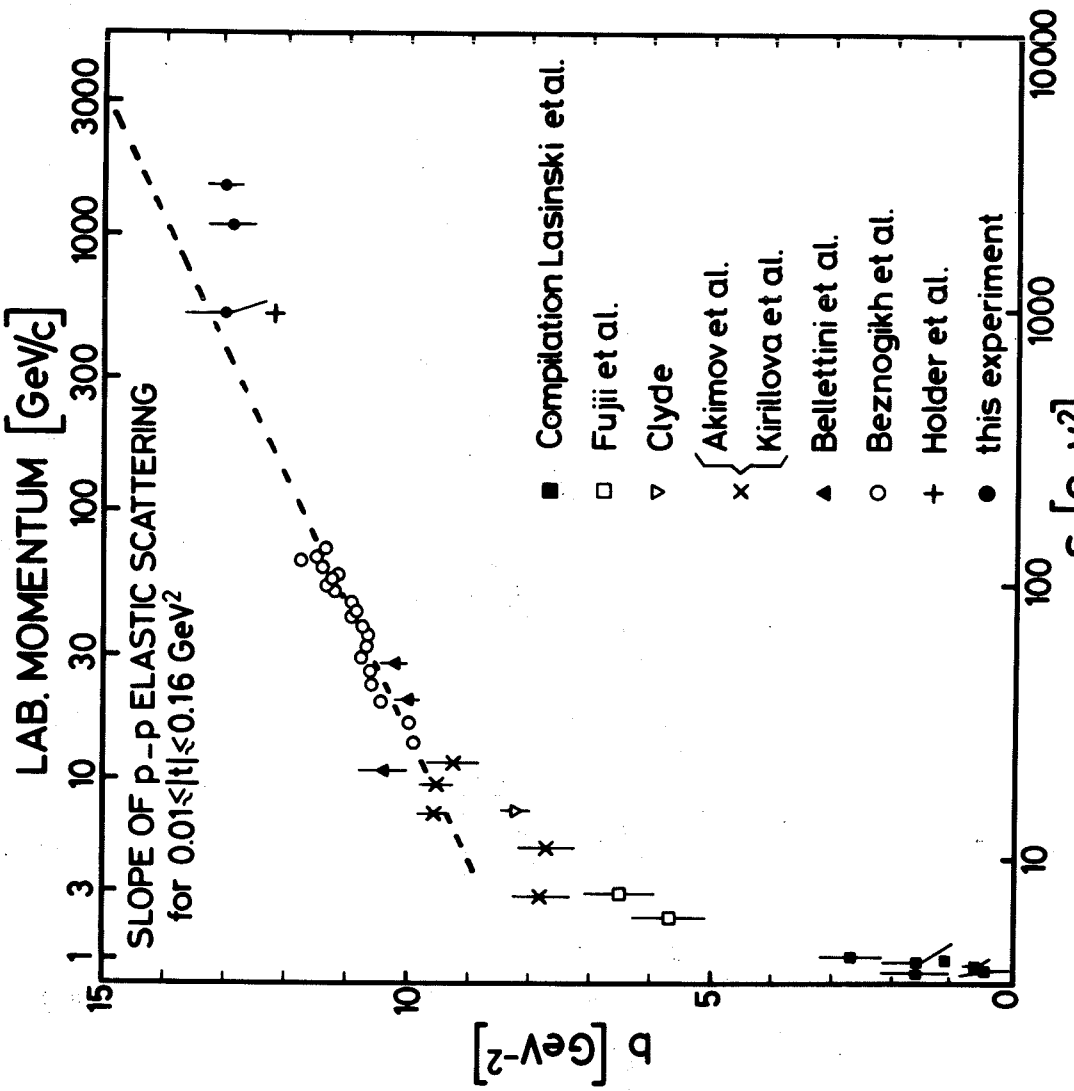
LAB. MOMENTUM [GeV/c]
SLOPE OF p-p ELASTIC SCATTERING
for 0.01≤|t|≤0.16 GeV²
b [GeV⁻²]
S [GeV²]
Compilation Lasinski et al.
Fujii et al.
Clyde
Akimov et al.
Kirillova et al.
Bellettini et al.
Beznogikh et al.
Holder et al.
this experiment

Fig. 16

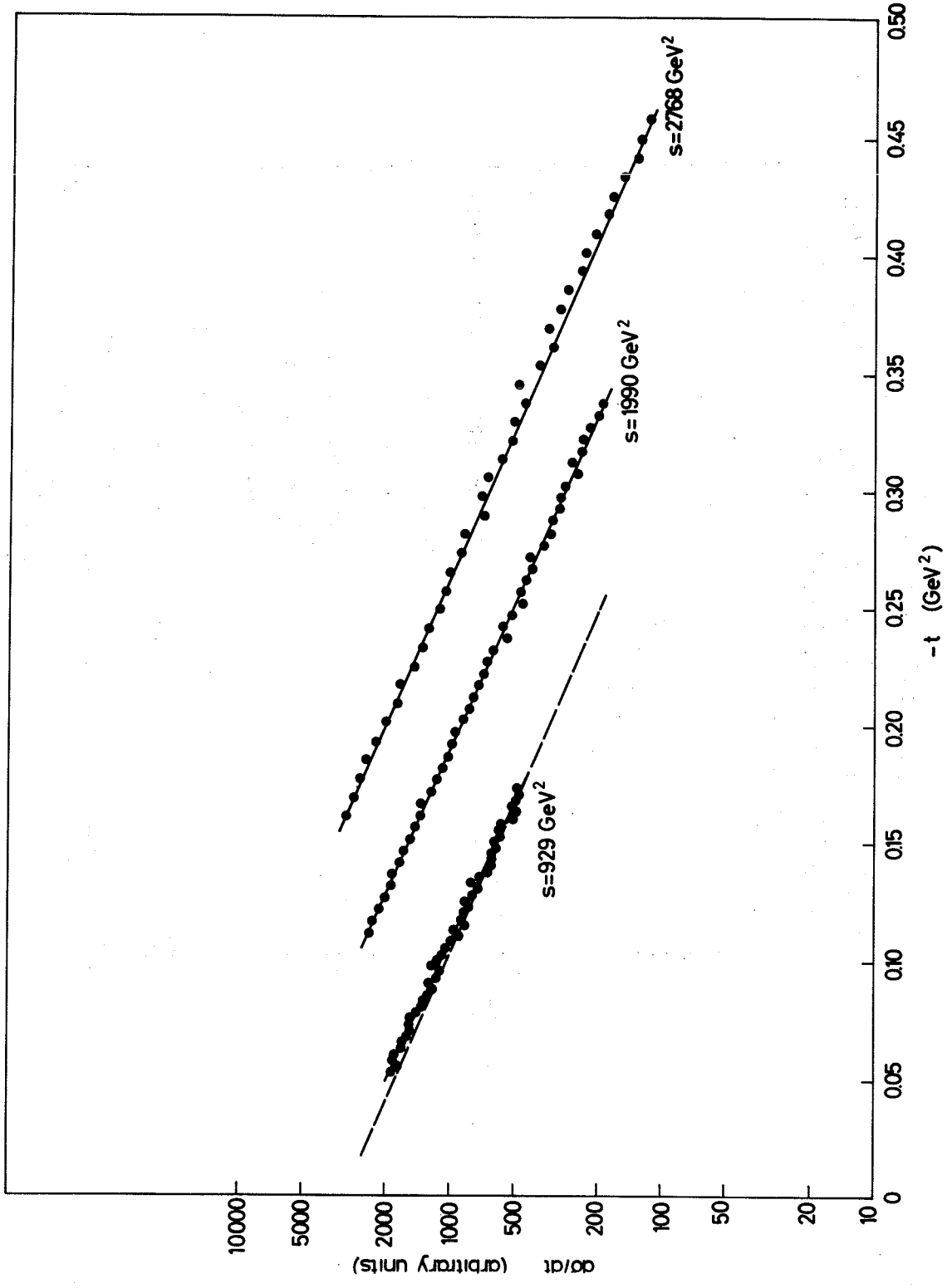
s=2768 GeV²
s=1990 GeV²
s=929 GeV²
dσ/dt (arbitrary units)
-t (GeV²)
10000
5000
2000
1000
500
200
100
50
20
10
0
0.05
0.10
0.15
0.20
0.25
0.30
0.35
0.40
0.45
0.50

Fig. 17

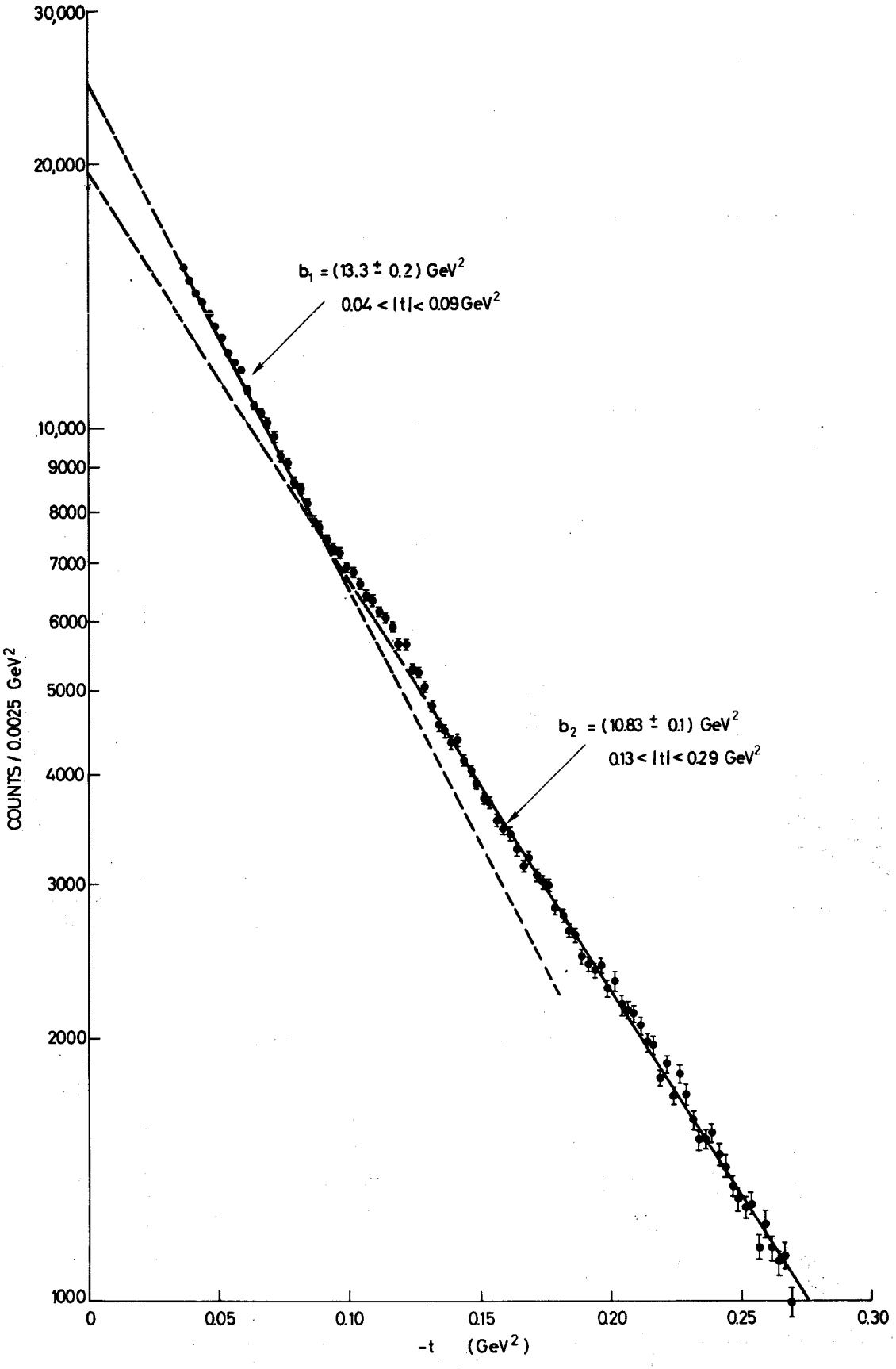
30,000
20,000
10,000
9000
8000
7000
6000
5000
4000
3000
2000
1000
COUNTS / 0.0025 GeV²
b₁ = (13.3 ± 0.2) GeV²
0.04 < |t| < 0.09 GeV²
b₂ = (10.83 ± 0.1) GeV²
0.13 < |t| < 0.29 GeV²
0
0.05
0.10
0.15
0.20
0.25
0.30
-t (GeV²)

Fig. 18

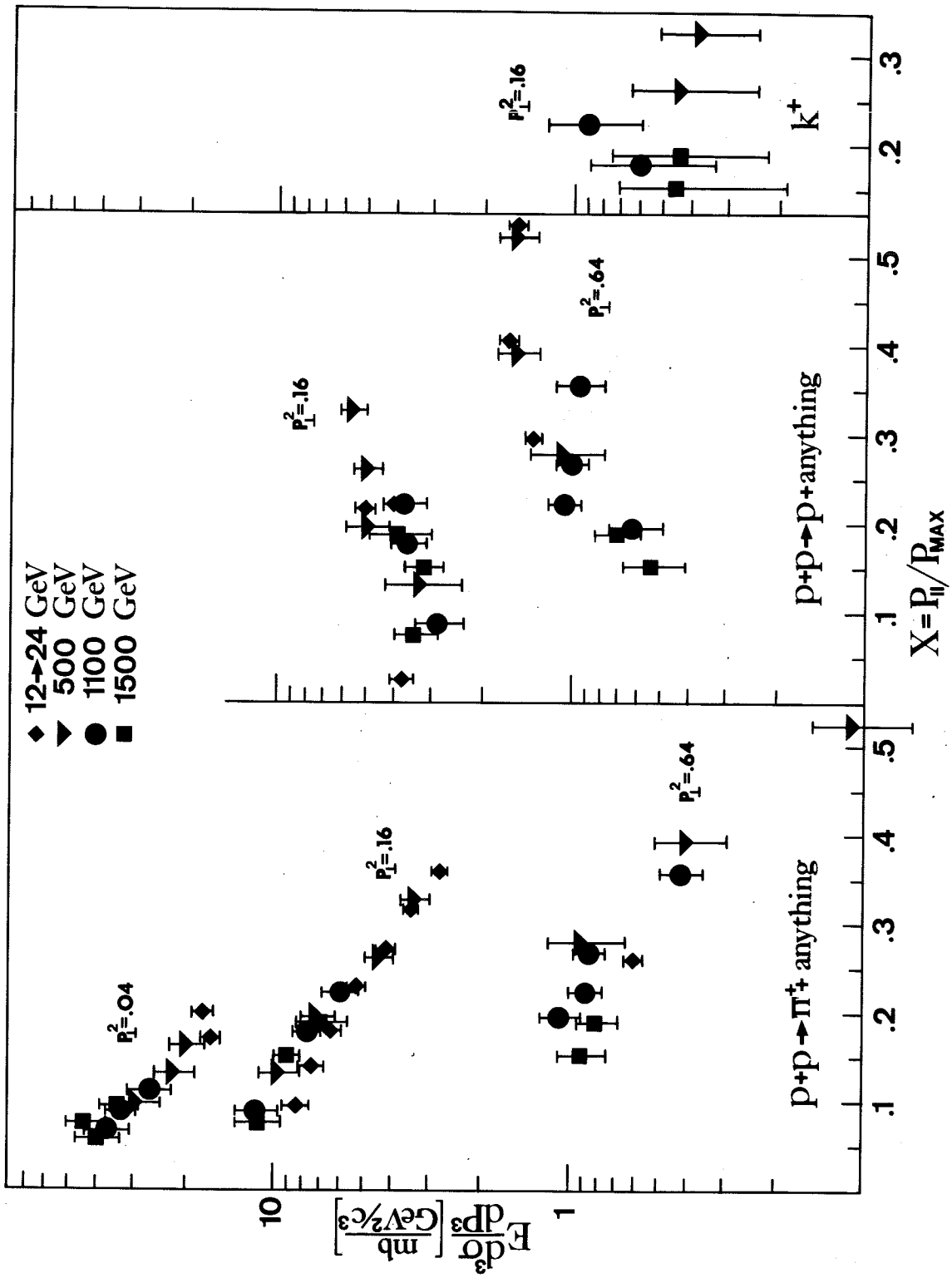
12→24 GeV
500 GeV
1100 GeV
1500 GeV
$E\frac{d^3\sigma}{dp^3}\left[\frac{mb}{GeV^2/c^3}\right]$
10
1
P_T^2=.04
P_T^2=.16
P_T^2=.64
p+p→π⁺ anything
p+p→p+anything
P_T^2=.16
P_T^2=.64
P_T^2=.16
K^+
.1
.2
.3
.4
.5
$X=P_{||}/P_{MAX}$

Fig. 19

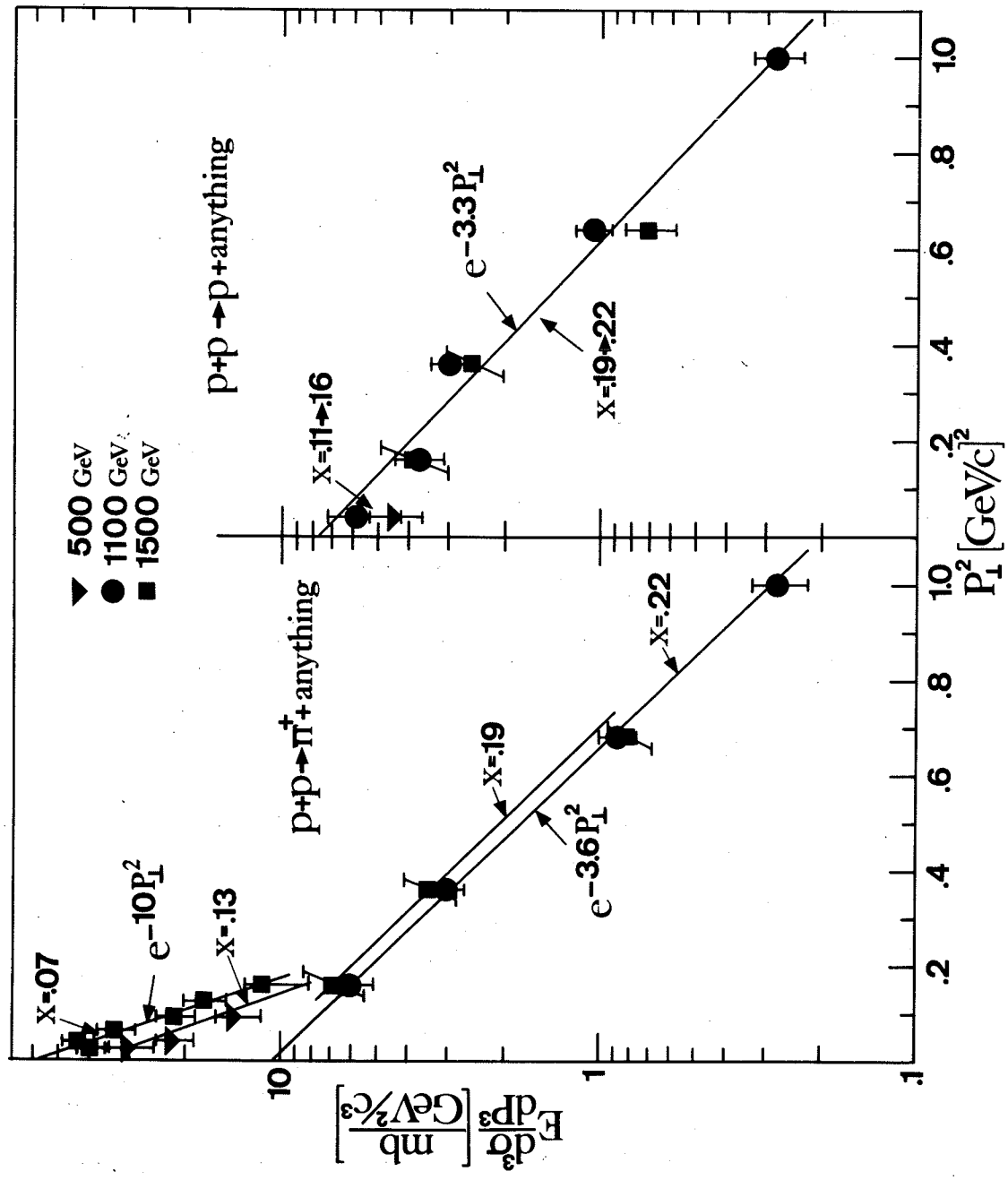
p+p→p+anything
p+p→π⁺+anything
500 GeV
1100 GeV
1500 GeV
x=.07
e^{-10P_T^2}
x=.13
x=.19
e^{-3.6P_T^2}
x=.22
x=.11→.16
e^{-3.3P_T^2}
x=.19→.22
E d³σ/dp³ [mb/GeV²/c³]
P_T² [GeV/c]²

Fig. 20

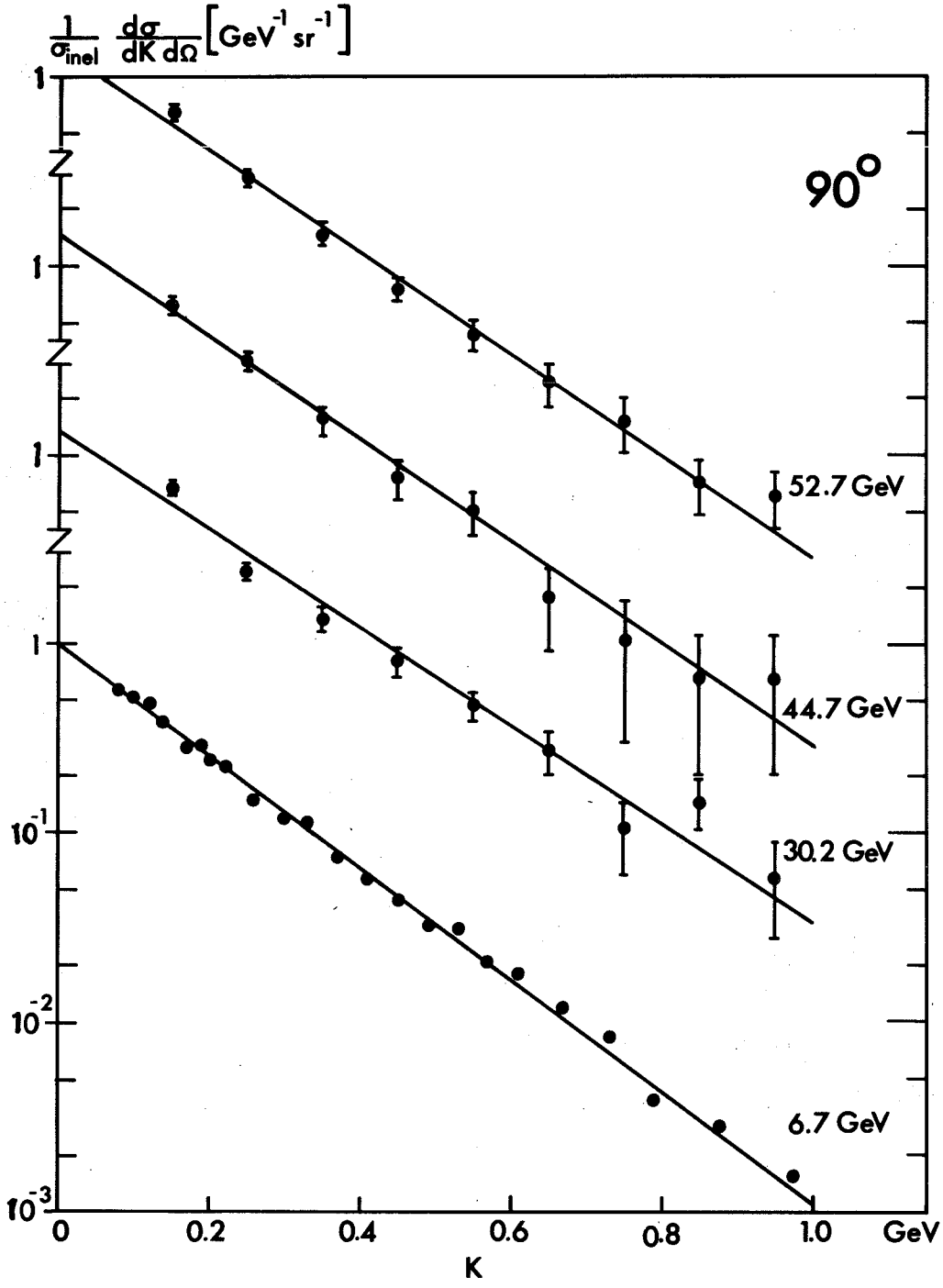
$\frac{1}{\sigma_{inel}} \frac{d\sigma}{dK\, d\Omega} [GeV^{-1} sr^{-1}]$
90°
52.7 GeV
44.7 GeV
30.2 GeV
6.7 GeV
1
1
1
1
10^{-1}
10^{-2}
10^{-3}
0
0.2
0.4
0.6
0.8
1.0
GeV
K

Fig. 21

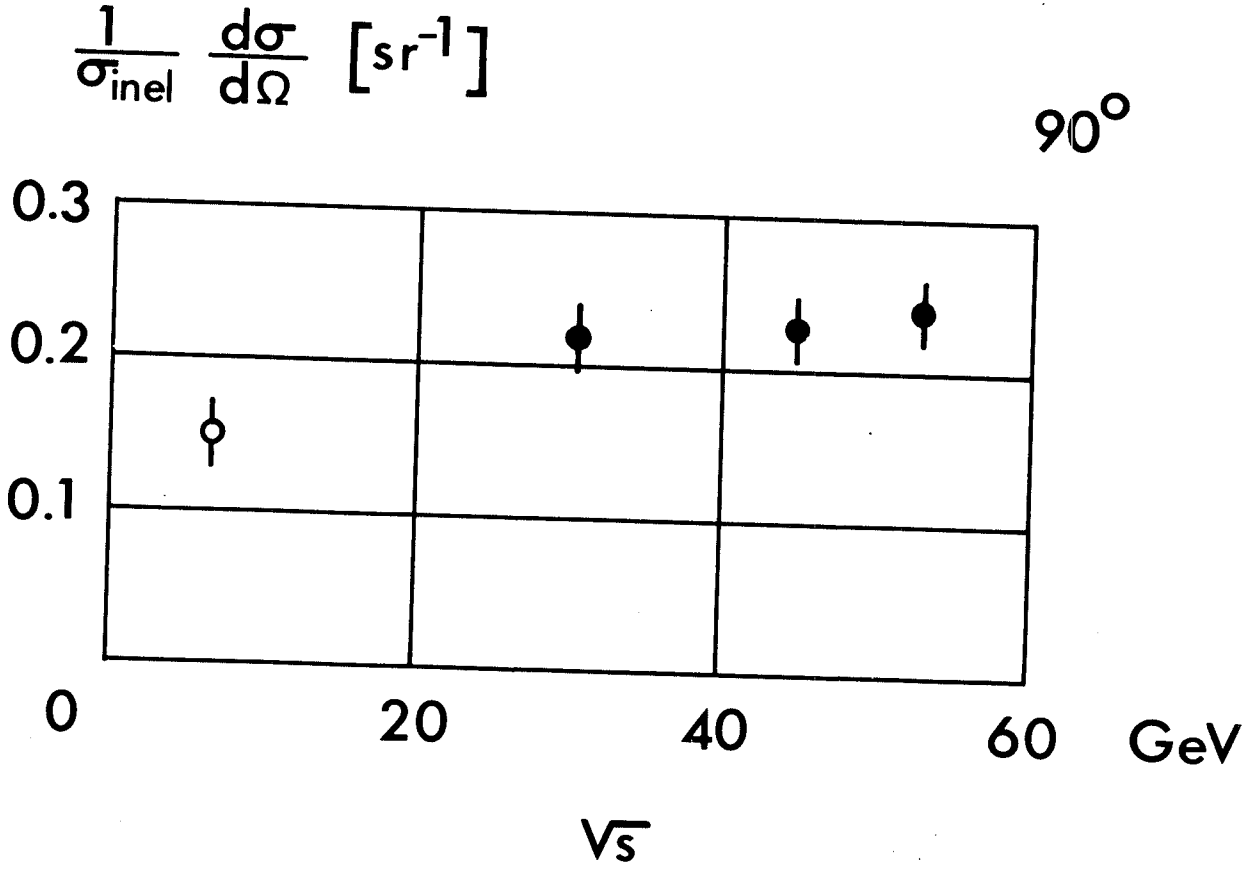
$\frac{1}{\sigma_{inel}} \frac{d\sigma}{d\Omega}$ [sr^{-1}]
90°
0.3
0.2
0.1
0
20
40
60
GeV
$\sqrt{s}$

Fig. 22